Winds and Eddy Dynamics in the Urban Canopy Layer over a City: a Parameterization Based on the Mixing-Layer Analogy

Lan Yao[1], Chun-Ho Liu[1,*], Guy P. Brasseur[2,3,4], and Christopher Y.H. Chao[5,6]

[1]Department of Mechanical Engineering, The University of Hong Kong, Hong Kong

[2]Department of Civil and Environmental Engineering, The Hong Kong Polytechnic University, Hung Hom, Kowloon, Hong Kong

[3]National Center for Atmospheric Research, Boulder, CO, USA

[4]Max Planck Institute for Meteorology, Hamburg, Germany

[5]Department of Building Environment and Energy Engineering, The Hong Kong Polytechnic University, Hung Hom, Kowloon, Hong Kong

[6]Department of Mechanical Engineering, The Hong Kong Polytechnic University, Hung Hom, Kowloon, Hong Kong

Revised Manuscript
Ref. No.: BAE-D-23-02938
submitted to
Building and Environment
on
October 10, 2023

**Corresponding author address:*
Chun-Ho LIU
Department of Mechanical Engineering
7/F, Haking Wong Building
The University of Hong Kong
Pokfulam Road, Hong Kong, CHINA
Tel: +852 3917 7901 / +852 9788 7951
Fax: +852 2858 5415
Email: liuchunho@graduate.hku.hk
https://aplhk.tech
ORCID: 0000-0002-4609-524X

Winds and Eddy Dynamics in the Urban Canopy Layer over a City: a Parameterization Based on the Mixing-Layer Analogy

Lan Yao[1], Chun-Ho Liu[1], Guy P. Brasseur[2,3,4], and Christopher Y.H. Chao[5,6]

[1]Department of Mechanical Engineering, The University of Hong Kong, Hong Kong

[2]Department of Civil and Environmental Engineering, The Hong Kong Polytechnic University, Hung Hom, Kowloon, Hong Kong

[3]National Center for Atmospheric Research, Boulder, CO, USA

[4]Max Planck Institute for Meteorology, Hamburg, Germany

[5]Department of Building Environment and Energy Engineering, The Hong Kong Polytechnic University, Hung Hom, Kowloon, Hong Kong

[6]Department of Mechanical Engineering, The Hong Kong Polytechnic University, Hung Hom, Kowloon, Hong Kong

Abstract

Urban atmospheric flows are vital to the global ecology. This study characterizes urban canopy layer (UCL) dynamics and parameterizes the flows in the atmospheric surface layer (ASL) over heterogeneous urban surfaces. Large-eddy simulations (LESs) are used to transiently calculate the winds over a real, dense city. A linear function of eddy diffusivity of momentum K_M is applied to the lower UCL. Analogous to its mixing-layer counterpart, the strong UCL top shear manifests an inflected mean wind speed profile which aligns well with the exponential law. The solutions to the mixing length l_m and the turbulent momentum flux are analytically derived by consolidating the mixing-layer type shear and the form drag from the explicitly resolved roughness elements. The behavior of l_m in the lower UCL, especially its peaked level, is captured well. Based on the balance between shear and form drag, an aerodynamic effective roof level H_{ae} is designated where the ground effect is alleviated under shear dominance. Results reveal that a rougher urban surface generates eddies with a larger shear length scale, thus enhancing momentum transport. In-canopy turbulence mixing, which slows wind decay, is also enhanced, resulting in stronger street-level breezes. The newly developed ASL flow model will be beneficial to urban planning by offering reliable predictions, thus effectuating the management of urban sustainability.

Word counts: 214

Keywords: exponential velocity profile; mixing-layer analogy; mixing-length parameterization; real urban morphology; urban canopy layer (UCL)

1. Introduction

Due to rapid urbanization, the ecological environment of cities is exerting an ever-growing influence on global hydrology and climate. The urban canopy layer (UCL) acts as an intimate medium for the exchange of momentum, heat, and mass between street canyons and the atmosphere (Mei and Yuan, 2022). The winds and turbulence within UCLs control environmental effects, such as greenhouse gas emission and urban heat island (UHI), which are crucial to urban precipitation and the hydrological cycle. It is therefore important to diagnose UCL flows over urban areas, especially megacities because of the dense population

(He et al., 2019) and the abundant anthropogenic emissions (Li and Wang, 2020).

Urban surfaces consist of irregular building layouts with a broad range of shapes, sizes, and orientations. Such a morphology inherently complicates the interaction between land surfaces and the atmospheric surface layer (ASL), triggering highly three-dimensional (3D), nonlinear turbulent flows (Liu et al., 2023b). To that end, this study strives to examine the winds and turbulent momentum fluxes of UCL flows over a real, dense city and parameterize the mixing length l_m and the turbulent momentum flux $u''w''$ (where double prime denotes the fluctuation from the mean, u the streamwise velocity, and w the vertical velocity). The outcome is important to climate management and meteorology applications, such as numerical weather predictions and air quality models (Vinayak et al., 2022).

The Prandtl mixing-length model is one of the classic turbulence closures for establishing the relationship between the turbulent momentum flux and mean velocity. Generally, the flows over canopies of porous media, for instance, vegetation, exhibit plane-mixing-layer behaviors that develop strong shear layers. The Kelvin–Helmholtz (K-H) instability induced characteristic eddies are estimated to be twice the shear length scale L_s (= $\langle \overline{u} \rangle / \left(d \langle \overline{u} \rangle / dz \right) \big|_{z=h}$ where h is the canopy height and u is the free-stream velocity) (Raupach et al., 1996). Here, overbars denote the resolved scales in the large-eddy simulation (LES) and angle brackets the ensemble average. The vortex flows govern the turbulence dynamics throughout the canopy (Finnigan, 2000). Accordingly, a natural assumption of constant l_m leads to an analytical urban canopy model (UCM) that yields the exponential mean wind speed

(MWS) profiles (exp-law; Raupach and Thom, 1981). The model robustness relies on the assumption of an invariant sectional drag coefficient C_d within the canopies. The model has been widely validated for ASL flows over plant canopies, such as cotton fields, maize crops, spruce, and pine forests (Ghisalberti and Nepf, 2006; Brunet, 2020), as well as aquatic flows over submerged vegetation (Ghisalberti and Nepf, 2002).

The applicability of the exp-law to UCL flows over inhomogeneous buildings is questionable. Unlike the momentum absorption by porous vegetation foliage, buildings exert stronger form drag (i.e., pressure difference between windward and leeward building facets) on the flows. Urban areas, thus, act as momentum sinks that lead to spectrum short-cut (Finnigan, 2000). Under this circumstance, the turbulence kinetic energy (TKE) of the dominant ASL eddies is circulated to the wake-scale vortices, resulting in rapid dissipation. Because of heterogeneity, buildings complicate wake generation in time and space. The resulting dynamics is hence fundamentally different from that over vegetation canopy. Although the invalidity of the exp-law was demonstrated based on the UCL flows over cuboids (Castro, 2017), the Prandtl mixing-length l_m is not a constant (Nezu and Sanjou, 2008; Theeuwes et al., 2019); instead, one or two local extremities appear in the canopies (Cheng and Yang, 2022). Additionally, studies have found that C_d decreases with increasing elevation z in UCLs for staggered arrays of cubes (plan area density λ_p = 0.25) with the same (Leonardi and Castro, 2010) or random height distribution (Xie et al., 2008).

Notwithstanding, the feasibility of exp-law has been verified by the UCL flows over arrays of densely packed, schematic roughness elements (frontal area density $\lambda_f = 0.56$; Huq et al., 2007), with uniform or non-uniform height distributions (Li et al., 2021). The drag induced by individual obstacles was reasonably parameterized using the exp-law (Yang et al., 2016). The exp-law model exhibited good agreement in the MWS profiles with the LES and DNS over staggered arrays of cubes within 40% UCL height (Cheng and Porté-Agel, 2021). Moreover, it well calculates well the shear strength, which is in line with those predicted by the conventional log-law at the canopy top (Macdonald, 2000). Although the constant l_m and the deduction of the UCL exp-law are dubious, the turbulence structures of similar scale to the canopy dominate momentum transport (Theeuwes et al., 2019).

Statistically, the turbulence quantities of flows over urban-like obstacles (e.g., rigid cylinders or cubes) resemble those of a plane mixing layer. The transport efficiency of the two types of flow peaks around the inflection point of MWS profiles ($r_{uw} = \langle u"w" \rangle / (\sigma_u \sigma_w) \approx -0.5$, where σ denotes the standard deviation). The momentum transport is more efficient than that of a smooth surface layer ($r_{uw} \approx -0.32$ in the inertial sublayer, ISL). Both UCL and mixing layer flows demonstrate non-Gaussian velocity distribution (magnitude of skewness $|Su| \approx O(1)$ and kurtosis $Ku > 3$; Böhm et al., 2013; Finnigan, 2000). Moreover, the maximum streamwise velocity fluctuations u" (i.e., turbulence intensity) of flows over urban-like obstacles are comparable to those of a plane mixing layer ($\sigma_u/u_* \approx 1.7$ where u_* is the friction velocity; Navok et al., 2000). The flow analogy between the UCL over real built surfaces and the mixing layer could be rationalized by the inflected MWS profiles collected from Basel (Giometto et al., 2016) and Guangdong (Cheng and Yang, 2022), the more efficient momentum transport in the upper roughness sublayer over Nanjing city (Zou et al., 2017), and the coherent structures in the non-Gaussian UCL flows over Seoul (Park et al., 2015; Han et al., 2017) and Kyoto (Yoshida et al., 2018). Hence, the mixing-layer analogy associated with the exp-law for UCL flows over real, dense cities merits further investigation to demystify the fundamental mechanism.

This study refines the mixing-layer analogy for the parametrization of UCL flows over a real, dense city using LES. This section introduces the problem background (Section 1). Following the methodology (Section 2), the eddy diffusivity (Section 3.1) and MWS profiles (Section 3.2) of UCL flows are parameterized. Afterward, a mixing-length model of the turbulent momentum flux is introduced and validated (Section 3.3). An analytical model for the eddy induced by two predominant forces is formulated (Section 3.4), after which the urban morphological effect is illustrated (Section 3.5). The practical implications are discussed (Section 4) before drawing the conclusions (Section 5).

2. Numerical method and model setup

The LES of the open-source CFD code OpenFOAM (2021), which is based on the Smagorinsky model (Smagorinsky, 1963), the SGS TKE conservation (Li et al., 2008), and the finite volume (FV) method, is adopted. Similar methods have been validated in our previous work on the ASL flows over schematic (Wong and Liu, 2013, Wu and Liu, 2018) and real (Liu et al., 2023a) urban morphologies. A systematic comparison between wind tunnel experiments and our LES methods has been reported (Mo and Liu 2023). The mathematical model and numerical method were detailed by Yao et al. (2022).

Kowloon Peninsula, Hong Kong (downtown area 4.4 × 4.4 km^2) is digitalized and the buildings are explicitly resolved (data source: the Survey and Mapping Office of Lands Department, HKSAR Government). Computation domain sizes 10 km (east-west) × 13 km (south-north) × 1 km (vertical; z) that is discretized into 26 million finite volume (FV) cells with grid stretching in the range of 1:4 –1:64. Hence, the characteristic size of the FV hexahedra is measured from 3 m to 50 m, and the Courant-Friedrichs-Lewy (CFL) number is kept less than 0.1 by setting the time increment $\Delta t = 0.01$ sec. The minimum grid spacing of FV cells follows the convention of 10% of the building length scale, which is in the range of 0.5 m –5 m (Tominaga et al., 2008). The LES first rans 6000 sec to initialize the ASL turbulence then another 7200 sec to achieve a quasi-steady state. Therefore, the total simulation time is $300H_a/u_*$. A background pressure gradient is prescribed such that the freestream wind speed U_∞ is approximately 10 m sec^{-1} from the south. The magnitude of the prescribed freestream velocity is determined by the field measurement of winds over Hong Kong (Lu and Sun, 2014), which agrees with the typical atmospheric boundary-layer flows (Hommema and Adrian, 2003), such as the flows over a compact built-up area of Seoul (9.5 m sec^{-1}; Park et al., 2015; Han et al., 2017), and the downtown Helsinki, Finland (10 m sec^{-1}; Auvinen et al., 2020). The Reynolds number Re (= $U_\infty H_{max}/\nu$; where H_{max} = 354 m is the height of the tallest building and $\nu = 1.56 \times 10^{-5}$ m^2 sec^{-1} the kinematic viscosity of air) is over 10^8 so the turbulent flows are fully developed (Elbing et al., 2011).

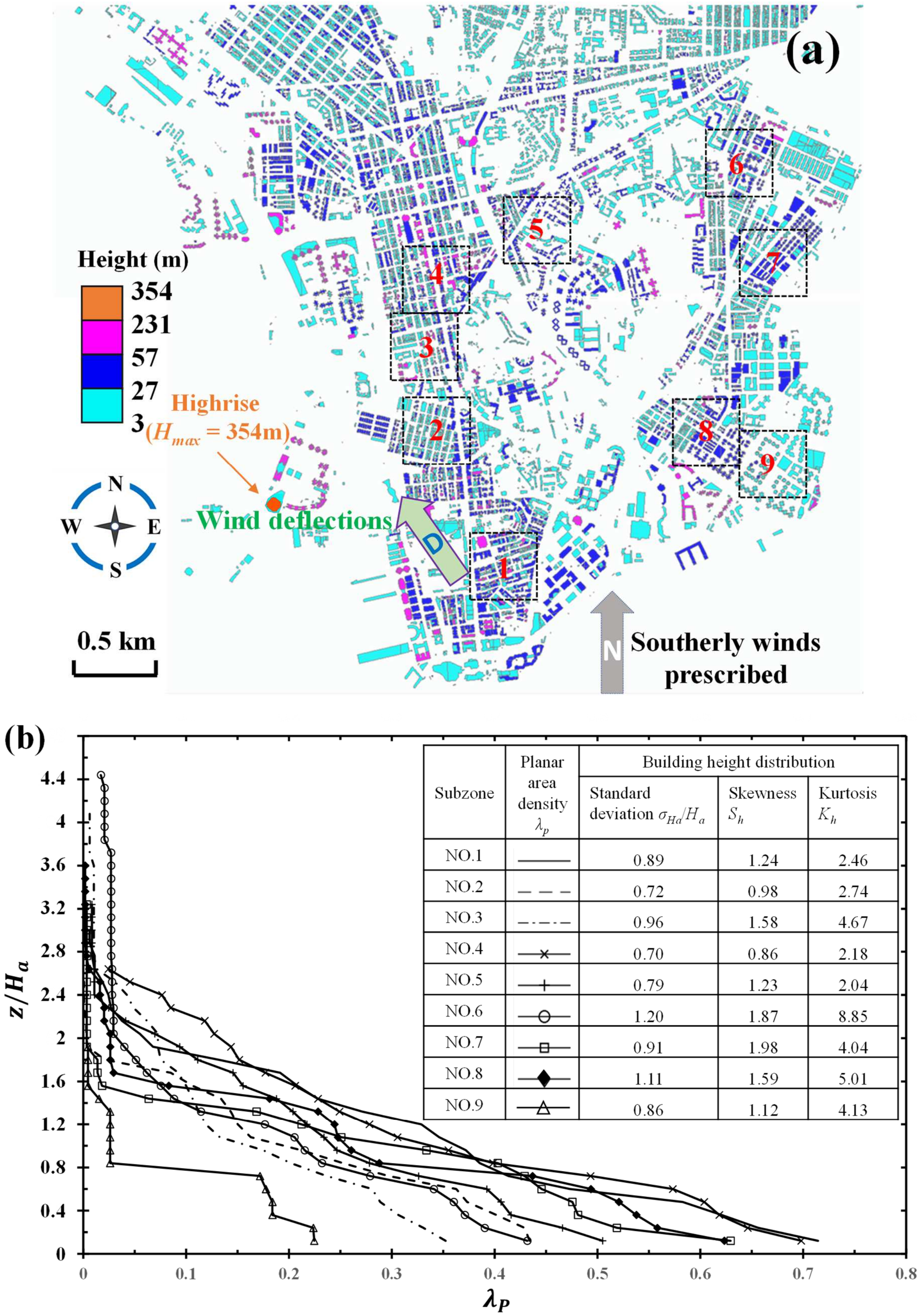

Subzone	Planar area density λ_p	Building height distribution: Standard deviation σ_{Ha}/H_a	Skewness S_h	Kurtosis K_h
NO.1	(solid line)	0.89	1.24	2.46
NO.2	(dashed line)	0.72	0.98	2.74
NO.3	(dash-dot line)	0.96	1.58	4.67
NO.4	(×)	0.70	0.86	2.18
NO.5	(+)	0.79	1.23	2.04
NO.6	(○)	1.20	1.87	8.85
NO.7	(□)	0.91	1.98	4.04
NO.8	(◆)	1.11	1.59	5.01
NO.9	(△)	0.86	1.12	4.13

Fig. 1. (a) Building height distribution in Kowloon Peninsula, HKSAR and (b) Statistics of building information and urban configuration.

Seven morphological indicators, namely the number of buildings N_b, plan area density λ_p, area-weighted H_a, and maximum H_{max} building height, together with the standard deviation σ_{Ha}, skewness S_h, and kurtosis K_h of building height, for the surface heterogeneity assessment are calculated for the geometric quantification of the urban surfaces. The projected area A_i of an individual building i is used for the calculation of λ_p (= $\sum_{i=1}^{N_b} A_i / A_l$), as is the height h_i for H_a (= $\sum_{i=1}^{N_b}(h_i A_i)/(\lambda_p A_l)$), considering the wind blockage by buildings. Accordingly, H_a is adopted for the 2nd (σ_{Ha}), 3rd (S_h), and 4th (K_h) moments of building height distribution. Specifically, K_h accounts for the influence of the minor but very tall buildings, which are crucial to the flow dynamics (Xie and Castro, 2009).

To characterize the UCL flows over dense urban areas with large spatial heterogeneity, nine subzones (individual lot area, A_l = 0.4 × 0.4 km^2) which present similar morphological features, i.e., the large height heterogeneity (building height distribution: kurtosis $K_h \geqslant 4$ for NO.3, NO.6 NO.7, NO.8, NO.9; normalized standard deviation $\sigma_{Ha} / H_a \geqslant 0.7$ for all) are selected. The numbering and geographical locations are depicted in Fig. 1a. The statistics of the building density and height distribution in each subzone are summarized in Fig. 1b. Given the asymmetric, massive building blockage, the prevailing winds are diverted from southerly to southeasterly. Hence, the new flow fields (velocity components and turbulent momentum fluxes) are post-processed for each subzone by the corresponding wind direction rotation $40^\circ \leq \Delta\Theta \leq 50^\circ$ counterclockwise from the south.

The following section parametrizes the wind and eddy dynamics of UCL flows. It first identifies the UCL and ISL, as well as diagnoses the aerodynamic properties of each subzone. In particular, eddy diffusivity is used to derive the analytical solutions to the mixing length and the turbulent momentum flux. Afterward, a UCL-flow model is formulated, and the building morphological factors are examined.

3. Theory

3.1 Eddy diffusivity

3.1.1 Characterization of ISL

According to K-theory, which is also known as flux-gradient diffusion (Schmidt, 1925), the turbulent momentum flux is driven by the velocity gradient

$$\langle u''w''\rangle(z) = -K_M(z)\frac{d\langle \overline{u}(z)\rangle}{dz} \quad (1)$$

where $K_M(z)$ is the eddy diffusivity. The Monin–Obukhov similarity theory (MOST; Monin and Obukhov, 1954) states that ASL eddies are self-similar. Additionally, the ISL eddy diffusivity

$$K_M^*(z) = \kappa u_*(z-d) \quad (2)$$

is proportional to the characteristic scales of velocity u_* and length $(z-d)$. Here, κ (= 0.42) is the von Kármán constant, d is the zero-plane displacement, and

$$u_* = \left(-\langle u''w''\rangle\big|_{\max}\right)^{1/2} \quad (3)$$

is the friction velocity which is calculated from the maximum downward turbulent momentum flux $-u''w''$ (Cheng and Castro, 2022).

Adopting the convention of constant-flux ISL, Eq. (1) to (3) are combined to yield the log-law velocity profile

$$\left\langle \overline{u}\left(z\right)\right\rangle = \frac{u_*}{\kappa}\ln\left(\frac{z-d}{z_0}\right) \tag{4}$$

where z_0 is the roughness length.

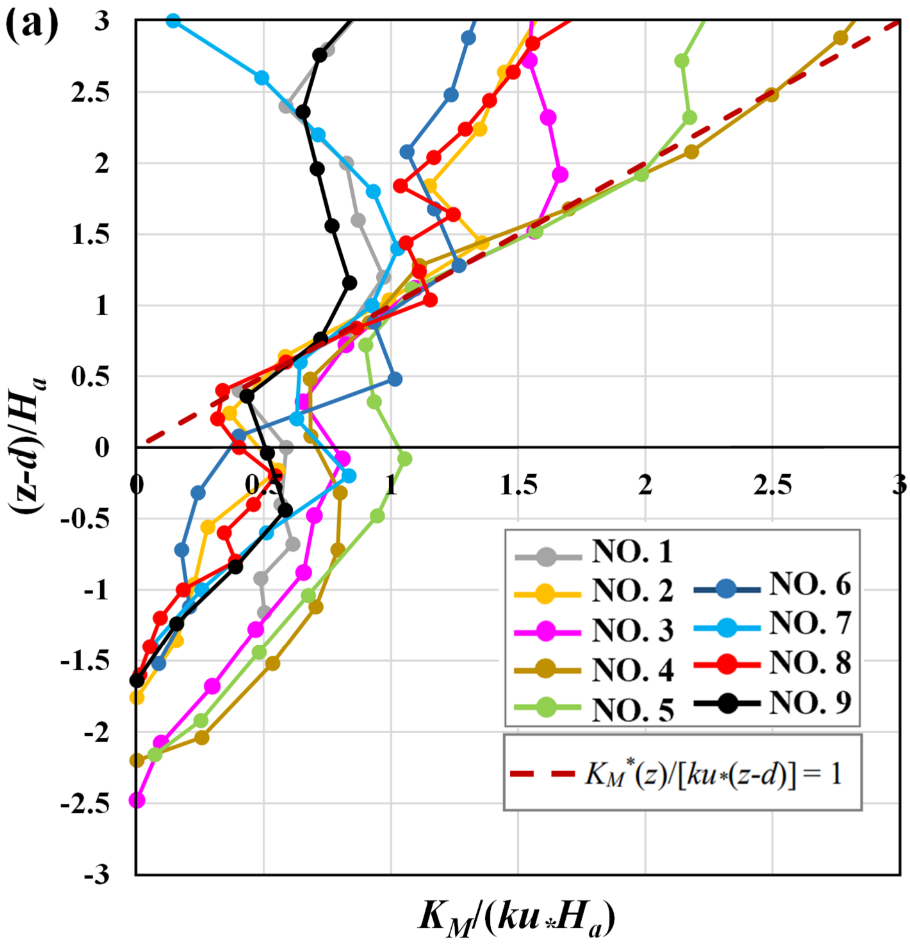

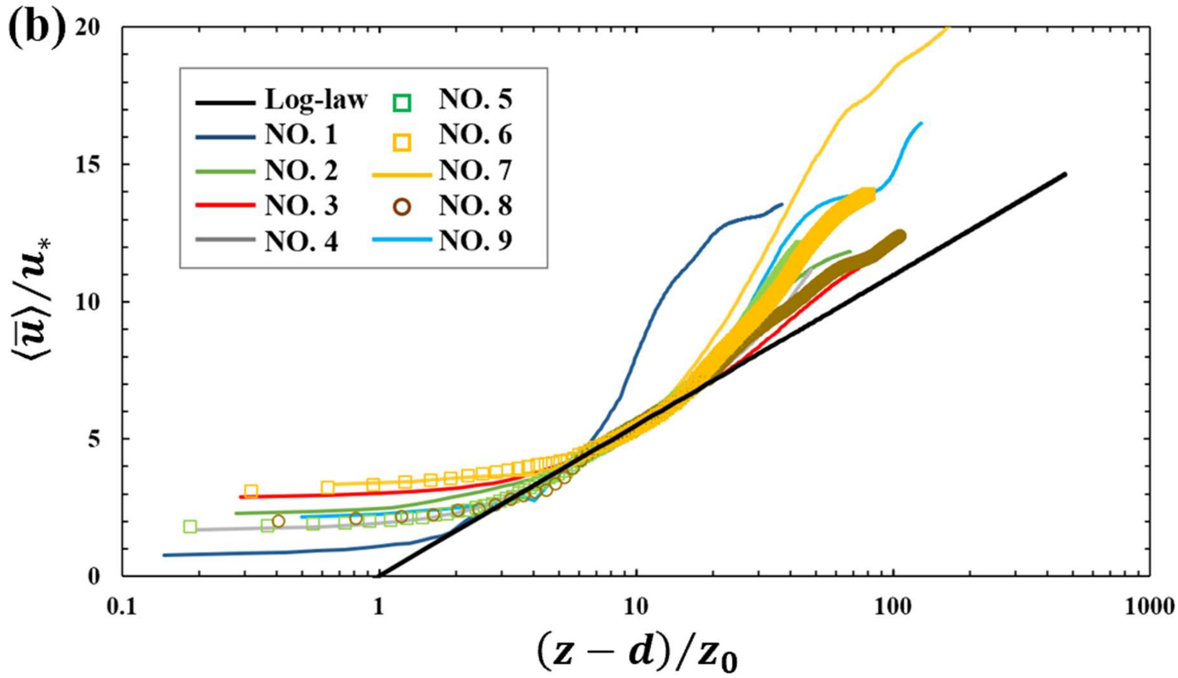

Fig. 2. Dimensionless profiles of (a) eddy diffusivity of momentum $K_M/\kappa u_* H_a$ plotted against displaced height $(z - d)/H_a$ and (b) mean wind speed (MWS) on semi-logarithmic plots.

For each subzone, Eq. (1) and (3) are applied to the ensemble-averaged (time- and horizontal-plane-averaged) LES datasets to obtain the vertical profile of $K_M(z)$ and the friction velocity u_*. According to Eq. (2), a linear regression is fitted to the LES-calculated $K_M(z)$. Next, the bottom and top boundaries of ISL and the zero-plane displacement d are determined by minimizing the root-mean-square errors (RMSEs). The roughness length z_0 is then determined by minimizing the RMSEs between the LES winds and those predicted by the log-law velocity profile Eq. (4). Further, the vertical profiles of LES-calculated $K_M(z)$ well align with the analytical solution Eq. (2) that outlines the ISLs of individual subzones (Fig. 2a).

The LES-calculated MWS profiles well collapse onto the log-law (Fig. 2b) that justifies the applicability of the K-theory for the ISL identification and the determination of ASL aerodynamic parameters (i.e., the levels of ISL boundaries, u_*, d, and z_0; Table 1) over diverse urban morphology. The rough surfaces benefit the turbulent momentum transport, featuring a large friction velocity 0.358 m $sec^{-1} \leqslant u_* \leqslant$ 0.685 m sec^{-1}, which agrees well with previous work by Mathis et al. (2009) (0.33 m $sec^{-1} < u_* <$ 0.96 m sec^{-1}) and Feigenwinter and Vogt (2005) (0.26 m $sec^{-1} < u_* <$ 0.70 m sec^{-1}). Among others, the subzones NO.2, NO.3, and NO.4 possess the largest friction velocity ($6.63 \times 10^{-2} \leq u_*/U_\infty \leq 6.85 \times 10^{-2}$), whereas the subzones NO.1, NO.7, and NO.9 possess the smallest friction velocity ($3.58 \times 10^{-2} \leq u_*/U_\infty \leq 5.57 \times 10^{-2}$).

3.1.2 Characterization of lower UCL

Below the zero-plane displacement d, K_M also demonstrates a vertical trend similar to that in the ISL, i.e., tends to linearly increase with increasing height (Fig. 2a). In this connection, a linear regression

$$K_{M-UCL}(z) = \kappa u_\tau (z - d_0) \tag{5}$$

is fitted to the LES datasets. Analogous to the momentum transport in ISL that is characterized by u_* and d, the characteristic velocity u_τ and displacement height d_0 are proposed for UCL flows.

The growth of eddy diffusivity $K_{M\text{-}UCL}$ in the UCLs is slower than that of K_M in the ISLs (Fig. 2a), suggesting a weaker turbulent mixing within. As tabulated in Table 1, the ratio of characteristic velocity scales falls into the range of 30% $\leq u_\tau/u_* \leq$ 70% (20% for NO.6), which represents the effective portion of turbulent momentum flux being transported from the ISLs deep into the UCLs.

Table 1. Summary of the characteristic parameters of the UCLs and ISLs.

Subzone	**Log-law**				**Exp-law**			
	ISL/H_a	**u_*/U_∞ (×10^{-2})**	**d/H_a**	**z_0/H_a (×10^{-1})**	**H_e/H_a**	**U_e/U_∞ (×10^{-1})**	**α**	**u_τ/u_***
NO. 1	2.48 to 3.20	5.57	1.92	2.74	2.48	1.03	3.9	N.A.
NO. 2	2.52 to 3.44	6.63	1.88	2.18	2.48	1.74	1.9	29.86%
NO. 3	3.16 to 4.20	6.85	2.52	1.13	3.48	3.38	2.0	42.62%
NO. 4	3.00 to 5.28	6.69	2.36	2.02	2.96	1.87	2.3	29.49%
NO. 5	3.24 to 4.76	6.18	2.48	2.18	3.24	1.88	2.3	55.89%
NO. 6	2.60 to 3.44	5.62	1.92	1.27	1.88	1.58	2.0	20.25%
NO. 7	1.88 to 2.40	3.58	1.60	0.60	2.20	1.93	3.4	69.34%
NO. 8	2.20 to 3.08	6.21	1.60	0.99	2.16	2.45	2.6	43.21%
NO. 9	2.16 to 2.68	4.65	1.80	0.80	2.20	1.72	3.0	51.20%

3.2 Identification and wind parameterization of UCL

3.2.1 UCL identification

ASL flows typically generate strong shear at the rooftop of identical obstacles (Reynolds and Castro, 2008). Such shear-characterized eddies govern the UCL dynamics. In the real urban context, flows impinge and separate vigorously at building edges, inducing appreciable drag. The wind shear exerted by heterogeneous buildings is calculated from the wind-speed gradient

$$\Omega(z) = \frac{d\left\langle \overline{u}(z) \right\rangle}{dz}, \tag{6}$$

which is crucial to UCL flow characterization.

It is reasonable to define the roof level as the UCL top for uniform roughness elements, such as homogeneous vegetation, two-dimensional ribs, or aligned arrays of 3D cubes. Notably, the UCL boundaries are erratic over surface heterogeneity. The UCL top of the cases reported in this study is defined at the elevation where the shear Ω peaks and the most vigorous turbulent transport arises. It coincides with the roof level over arrays of identical obstacles (Macdonald, 2000). In response to the flow discontinuity and K-H instabilities, the MWS profiles are inflected at the UCL top (Zhao et al., 2023; Alwi et al., 2023). This level and the associated velocity are denoted as H_e and U_e, respectively (Table 1).

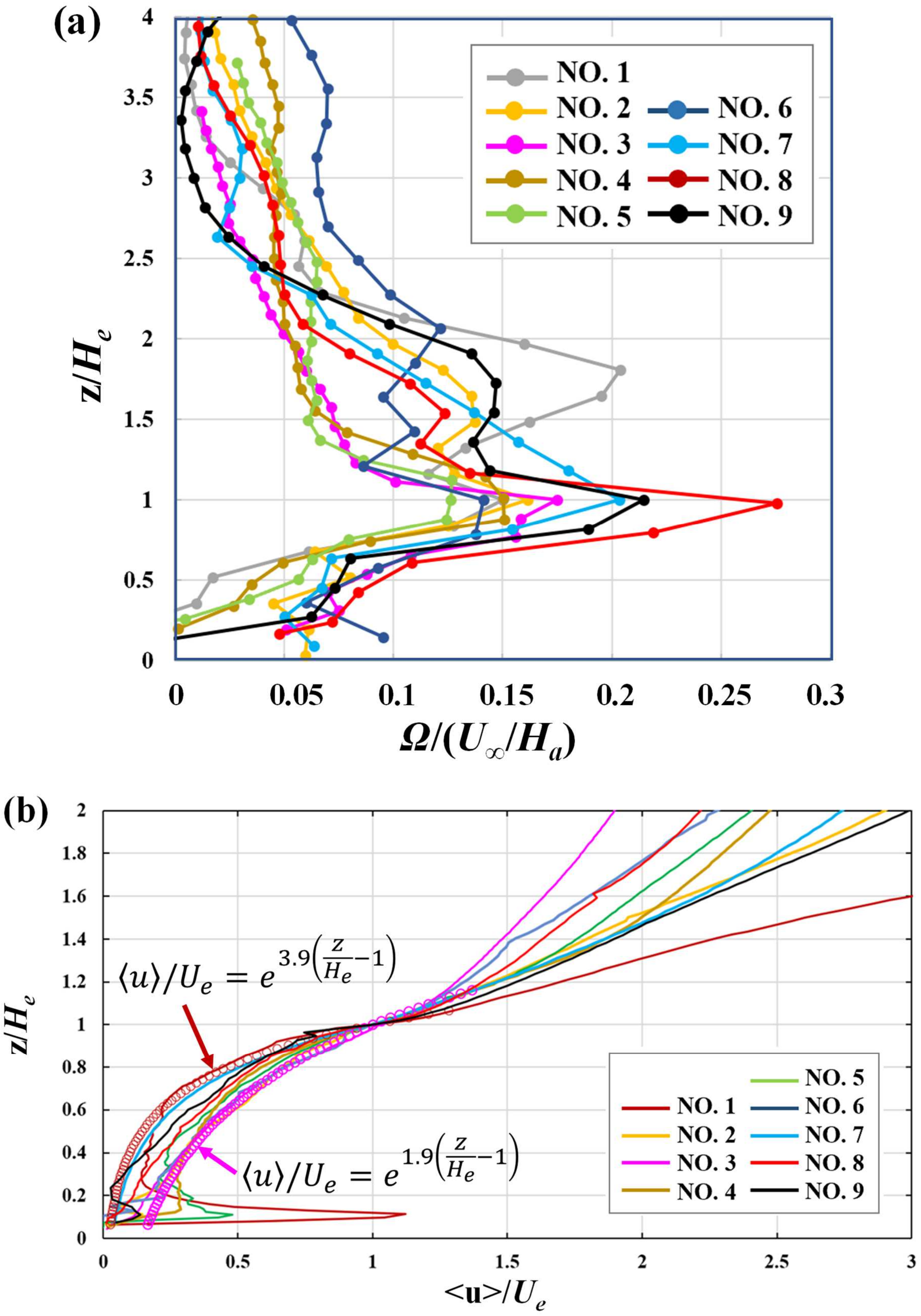

Fig. 3. Dimensionless (a) wind shear $\Omega(z)/(U_\infty/H_a) = \left(d\left\langle \overline{u}(z)\right\rangle/dz\right)/(U_\infty/H_a)$ and (b) mean-wind speed $\left\langle \overline{u}(z)\right\rangle/U_e$ plotted against dimensionless height, z/H_e.

The wind shear apparently increases with increasing elevation, which rapidly reaches a remarkable magnitude at $z = H_e$ (Fig. 3a), denoting a strong shear layer developed over the building roof ($H_a \approx 25$ m; $H_e > H_a$; Table 1). Such shear determines an inflection on the MWS profiles (Fig. 3b), which is strongest in the subzones with exceptional building heterogeneity ($K_h > 3$), namely NO.3, NO.7, NO.8, and NO.9. Despite the less intense wind shear peaking at $z = H_e$ in NO.6, its most heterogeneous building configuration ($K_h > 8$) boosts the maximum wind shear to a higher elevation above $2H_e$.

3.2.2 MWS profile parameterization

The shear-characterized MWS profiles are analogous to their mixing-layer flow counterparts. Moreover, the characteristic eddies, whose size is comparable to that of the roughness elements, dominate the dynamics throughout the UCLs. For a plane mixing layer, the vorticity thickness is twice the shear length scale at the UCL top (Raupach et al., 1996)

$$L_{s-C}(z) = \frac{\langle \bar{u}(z) \rangle}{d\langle \bar{u}(z) \rangle / dz}, \tag{7}$$

which is determined by the velocity and wind-shear strength at the inflection (Poggi et al., 2004). Similar to recent findings (Xie et al., 2008; Li et al., 2021), the current LES wind data resemble the exp-law (exponential profile; Fig. 3b), such that

$$\langle \bar{u}(z) \rangle = U_e e^{\alpha(z/H_e - 1)}. \tag{8}$$

Moreover, the wind-shear strength of the exp-law profile is given by

$$\Omega(z) = \frac{d\langle \bar{u}(z) \rangle}{dz} = \frac{\alpha}{H_e} U_e e^{\alpha(z/H_e - 1)}. \tag{9}$$

Combing Eq. (7) and (9) yields the shear length scale of mixing-layer flows

$$L_{s-ML} = \frac{U_e e^{\alpha(z/H_e - 1)}}{\frac{\alpha}{H_e} U_e e^{\alpha(z/H_e - 1)}} = \frac{H_e}{\alpha}, \tag{10}$$

where α is an empirical constant known as the attenuation coefficient, representing the wind decay rate in UCLs. Systematic studies have suggested that α is closely related to surface morphological features, such as cuboid density (Macdonald, 2000). In the current study, α is determined for each subzone by minimizing the RMSEs of the regression between the analytical solution (Eq. 8) and the LES-calculated MWS (Table 1). Notably, for plane-mixing-layer flows, the shear length scale $L_{s\text{-}ML}$ only depends on H_e and α.

The UCL MWS profiles of all the subzones are enveloped by two exponential models (Eq. 8; α = 1.9 and 3.9; Fig. 3b). Moreover, the MWS profiles decay exponentially during the descent into canopies. Noticeable deviations of MWS profiles from the exp-law are observed at street level due to the complex flows at the UCL bottom, such as flow channeling by the main streets with wide openings or flow recirculation by building sheltering. Therefore, strong winds, for example, at the bottom 20% UCLs of subzones NO.1, NO.5, and NO.4, or reverse flows ($z \leq 0.1H_e$) (Castro, 2017; Nagel et al., 2023), could be observed.

The wind decay is fastest ($1.9 \leq \alpha \leq 2.0$; $5.62\times10^{-2} \leq u_*/U_\infty \leq 6.85\times10^{-2}$) in subzones NO.2, NO.3, and NO.6but slowest ($3.0 \leq \alpha \leq 3.9$; $3.58 \leq u_*/U_\infty \leq 5.57$) in subzones NO.1, NO.7, and NO.9. The rougher surfaces, which could deliver more turbulent momentum flux, result in faster winds within canopies but with slower winds above the UCLs. To evaluate the capability of the exp-law for shear calculation, two shear length scales, the analytical $L_{s\text{-}ML}$ (= H_e/α; Eq. 10) based on mixing-layer flows and the LES-calculated $L_{s\text{-}C}$ (Eq. 7), are compared. The results demonstrate that the exp-law model well predicts the shear length scale at the UCLs top ($0.89 \leq L_{s\text{-}ML}/L_{s\text{-}C} \leq 1.09$; Table 2).

Table 2. Summary of dimensionless inflection height, H_e/H_a, mixing-layer shear length scale, $L_{s\text{-}ML}/H_a$ (Eq. 10), LES-calculated shear length scale, $L_{s\text{-}C}/H_a$ (Eq. 7), and the length-scale ratio $L_{s\text{-}C}/L_{s\text{-}ML}$.

Subzone	**UCL height**	**Shear length scale**		**Length-scale ratio**
	H_e/H_a	**Theoretical mixing-layer** $L_{s\text{-}ML}/H_a = H_e/(\alpha H_a)$	**LES-calculated** $L_{s-C}/H_a = \left(\langle \bar{u} \rangle / \left(d\langle \bar{u} \rangle / dz \right)\Big|_{z=H_e} \right) / H_a$	$R_s = L_{s\text{-}C}/L_{s\text{-}ML}$
NO. 1	2.48	0.64	0.57	89.63%
NO. 2	2.48	1.28	1.24	97.34%
NO. 3	3.48	1.74	1.63	93.86%
NO. 4	2.96	1.29	1.19	92.22%
NO. 5	3.24	1.31	1.26	96.33%
NO. 6	1.88	0.87	0.90	102.83%
NO. 7	2.20	1.23	1.20	97.31%
NO. 8	2.16	0.82	0.80	97.97%
NO. 9	2.20	0.74	0.80	109.21%

3.3 Mixing length model and parameterization of UCL turbulent momentum flux

3.3.1 Mixing length model

The uncertainty of the two assumptions associated with vegetative canopies is the primary concern when assessing the applicability of the exp-law to UCL flows over obstacles. In this section, we derive the mixing length from the exp-law for UCL MWS profiles and the empirical UCL eddy diffusivity functions to verify the newly proposed parameterizations.

According to the Prandtl mixing length model, the mixing length $l_m(z)$ is governed by

$$-\langle u''w''\rangle = l_m^2(z)\left(\frac{d\langle \bar{u}(z)\rangle}{dz}\right)^2. \tag{11}$$

Comparing with Eq. (1) yields

$$l_m^2(z) = \frac{K_M(z)}{d\langle \bar{u}(z)\rangle / dz}. \tag{12}$$

Applying the linear eddy diffusivity (Eq. 5) and the exponential velocity function (Eq. 7) leads to the analytical UCL mixing length

$$l_{m-UCL}^2(z) = \frac{K_{M_{UCL}}(z)}{d\langle \bar{u}(z)\rangle / dz} = \frac{\kappa u_\tau (z-d_0)}{\alpha / H_e \times U_e e^{\alpha(z/H_e - 1)}}. \tag{13}$$

As shown in Eq. (13), the mixing length l_{m-UCL} is far from constant. Instead, considering both the ground surface and the shear generated right over the UCL, which are in balance, justifies the rationality of the parameterization. In the descent into the UCLs, the winds slow down and vanish on the ground surface, exerting friction drag on the flows. Such effects on mixing length are analogous to the self-similarity of eddy organization theory (Poggi et al., 2004). Analytically, the eddy mixing length in the ASL is proportional to the wall-normal distance. Likewise, the ground effect is parameterized as the linear eddy diffusivity term $\kappa u_\tau(z - d_0)$ in the numerator of Eq. (13), which is in line with the standard ASL parameterization (MOST; Monin and Obukhov, 1954). On the other hand, the denominator of Eq. (13) $\alpha/H_e \times U_e e^{\alpha(z/He-1)}$ represents the strong shear that endows the turbulent eddies with the mixing-layer type eddy diffusivity. It is proportional to the velocity gradient by a factor of square of (α/H_e) at the UCL top.

The influence of the ground surface on the eddy diffusivity is governed by

$$K_{M-ground}\left(z\right)=\kappa u_\tau\left(z-d_0\right). \quad (14)$$

The mixing length in mixing-layer flows equals the shear length scale at the inflection, i.e., $l_{m-ML} = L_{s-ML} = H_e/\alpha$ (Eq. 10; Poggi et al., 2004). Therefore, the eddy diffusivity due to shear is

$$K_{M-shear}\left(z\right)=l_{m-ML}^2\frac{d\left\langle \overline{u}\left(z\right)\right\rangle}{dz}=\frac{H_e}{\alpha}U_e e^{\alpha\left(z/H_e-1\right)}. \quad (15)$$

Consolidating Eq. (13), (14), and (15), the UCL mixing length is rewritten in the form

$$l_{m-UCL}\left(z\right)=\frac{H_e}{\alpha}\times\sqrt{\frac{K_{M-ground}\left(z\right)}{K_{M-shear}\left(z\right)}}. \quad (16)$$

Note that $l_{m-UCL}(z)$ is close to zero and H_e/α, respectively, approaching the ground and the UCL top. Therefore, the non-zero exponential term ($K_{M-shear} > 0$) is the denominator in Eq. (16), whereas the linear $K_{M-ground}$ is the numerator, which is zero at the ground. Additionally, shear gradually comes to dominate further from the ground. By contrast, the effect of ground surface is weakened because the exponential term intrinsically increases faster than the linear term. This is natural because the special, extreme "chopstick-like" urban morphology impedes the eddy descent into the canopies immediately after their generation around the UCL top.

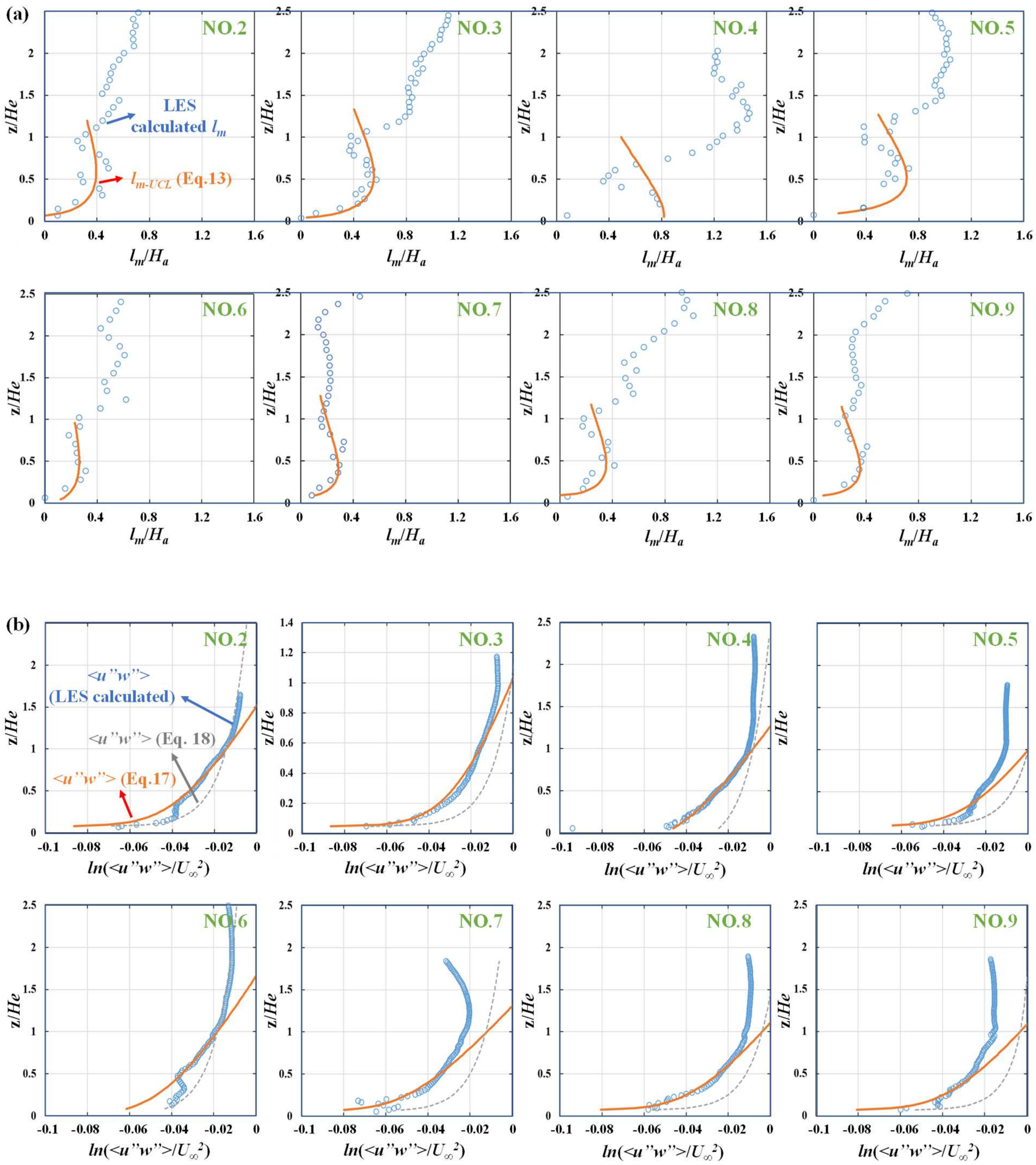

Fig. 4. Dimensionless (a) mixing length l_m/H_a and (b) turbulent momentum flux $ln(<u''w''>/U_\infty^2)$ plotted against dimensionless height z/H_e.

Notably, the validity of the linear eddy diffusivity of the turbulent momentum flux $K_{M\text{-}UCL}$ (Eq. 5) could be retained within most of the canopies (up to $z = 0.8H_e$; Fig. 5). Accordingly, the LES-calculated l_m (Eq. 11) generally follows the vertical tendency of the mixing-length model (Eq. 13 and 16) in such a vertical zone (Fig. 4a). Moreover, the model can capture the peaked mixing length near $z = 0.5H_e$. The flows in NO.1 are complicated, such as the gusts and the negative wind-speed gradient at the bottom UCL, resulting in an invalid l_m (Table 1). Nonetheless, the model is applicable to for predicting l_m for real urban winds.

3.3.2 Parameterization of UCL turbulent momentum flux

Consolidating Eq. (8), (11), and (13) yields the analytic turbulent momentum flux in logarithmic form

$$\ln\left(-\langle u''w''\rangle\right) = \ln\left(z - d_0\right) + \alpha\left(z/H_e - 1\right) + \ln\left(\frac{\kappa u_\tau \alpha}{H_e} U_e\right). \qquad (17)$$

Within the UCL ($d_0 \leq z \leq H_e$), the linear UCL top shear $\alpha(z/H_e - 1)$ intrinsically increases faster than does the logarithmic ground effect $\ln(z - d_0)$ in Eq. (17). Therefore, the UCL top shear dominates the modification of the momentum flux. On the other hand, the UCL top shear is negligible near the ground surface $z \approx 0$ so Eq. (17) is simplified to

$$\ln\left(-\langle u''w''\rangle\right) = \ln\left(z - d_0\right) + \ln\left(\frac{\kappa u_\tau \alpha}{H_e} U_e\right). \qquad (18)$$

These two momentum flux models, Eq. (17) and (18), are compared with the LES datasets for each subzone (Fig. 4). Although the UCL-top shear is dropped, Eq. (18) predicts satisfactorily the vertical momentum flux at the bottom UCLs (Fig. 4b) for all the subzones except NO.4, demonstrating the dominance of the near-ground modification term $\ln(z - d_0)$. When moving from the ground, in contrast, the discrepancy between Eq. (18) and the LES-calculated momentum flux increases. However, when the UCL-top shear $\alpha(z/H_e - 1)$ is included, Eq. (17) exhibits a good fit for most UCLs. This implies that the shear layer changes the turbulent momentum flux substantially, modifying the momentum transport. In particular, the urban morphology of NO.4 features very dense but rather uniform high-rise buildings ($\lambda_p \approx 0.7$, $K_h < 3$, $\sigma_{Ha}/H_a \approx 0.6$; Fig.1b) that helps preserve the UCL-top-generated shear in the deep urban canopies and even near the ground surface at $z \approx 0$. Hence, the shear-layer dynamics is nonnegligible in land-surface parameterization.

To further investigate how deep the UCL-top shear affects canopy flows (i.e., the linear term $\alpha(z/H_e - 1)$ in Eq. 17), the vertical profiles of the LES-calculated shear length scale (Eq. 7) are plotted in Fig. 6. As shown in Fig. 6b, at 60% depth in UCLs, the shear length scale $L_s(z)$ is 60% of its UCL-top counterpart $L_s(H_e)$. Specifically, the stronger the UCL-top shear is (longer $L_s(H_e)$), the deeper the penetration into UCLs. Taking NO.3 as an example, assume $0.7L_s(H_e)$ ($L_s(H_e) \approx 1.9H_a$) spans a vertical extent of $0.75H_e$ down from the UCL top. Therefore, the dominant eddies are more uniform in size vertically in the UCLs of the heterogeneous real urban morphology than those over homogeneous vegetations (Thomas and Foken, 2007) or schematic roughness elements (Castro et al., 2006). Moreover, the ratio of $L_s(H_e)$ to H_a is in the range of $0.6 \le L_s(H_e)/H_a \le 1.9$, which is comparable to that of vegetations ($0.3 \le L_s(H_e)/H_a \le 0.9$; Finnigan, 2000) and urban-like canopies ($0.4 \le L_s(H_e)/H_a \le 1.3$; Novak et al., 2000). Such a uniform vertical distribution of eddies augments UCL momentum transport and mixing, leading to windier in-canopy flows.

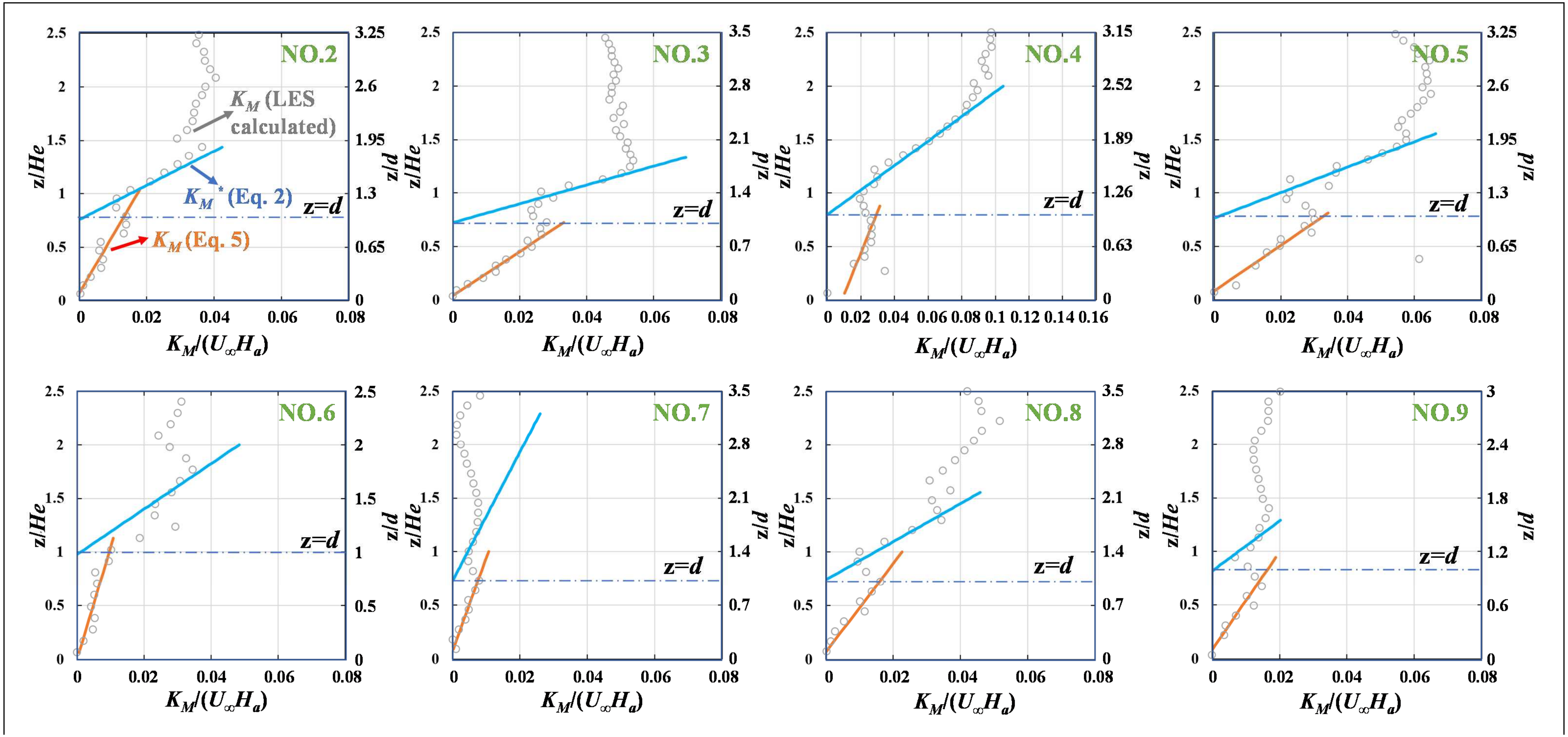

Fig. 5. Dimensionless eddy diffusivity of momentum $K_M/(U_\infty H_a)$ plotted against dimensionless height z/H_e.

The dominance of the mixing-layer type eddies within UCLs further demonstrates the validity of the exponential MWS profiles (Eq. 6) for in-canopy flows. The assumption of invariant mixing length and sectional drag, which is the basis of the exp-law for homogeneous vegetation canopies is, however, inadequate to refute the efficacy of the exp-law for heterogeneous rough surfaces.

3.4 A model of UCL flows

3.4.1 Zero-plane displacement *d*

In Section 3.1, the roughness length z_0 and zero-plane displacement d of ISLs are determined using the linear relationship between eddy diffusivity of momentum and displaced height $K_M^*(z) = \kappa u_*(z - d)$; Eq. 2. For regular arrays of urban-like, identical cuboids (Reynolds and Castro, 2008) or vegetation canopies (Macdonald, 2000; Brunet, 2020), d is generally lower than the roof level (mean roughness height, H_a), implying that the drag center is mostly submersed in the UCL. Moreover, the turbulence structures are more coherent and active within UCLs than those above although the effect of surface roughness extends above the roof level to $3H_a \leq z \leq 5H_a$ (Zhu et al., 2017). In this connection, d plays the important role of characterizing rough-surface flows and is adopted as the average elevation of momentum absorption in ASL flows (Thom, 1971).

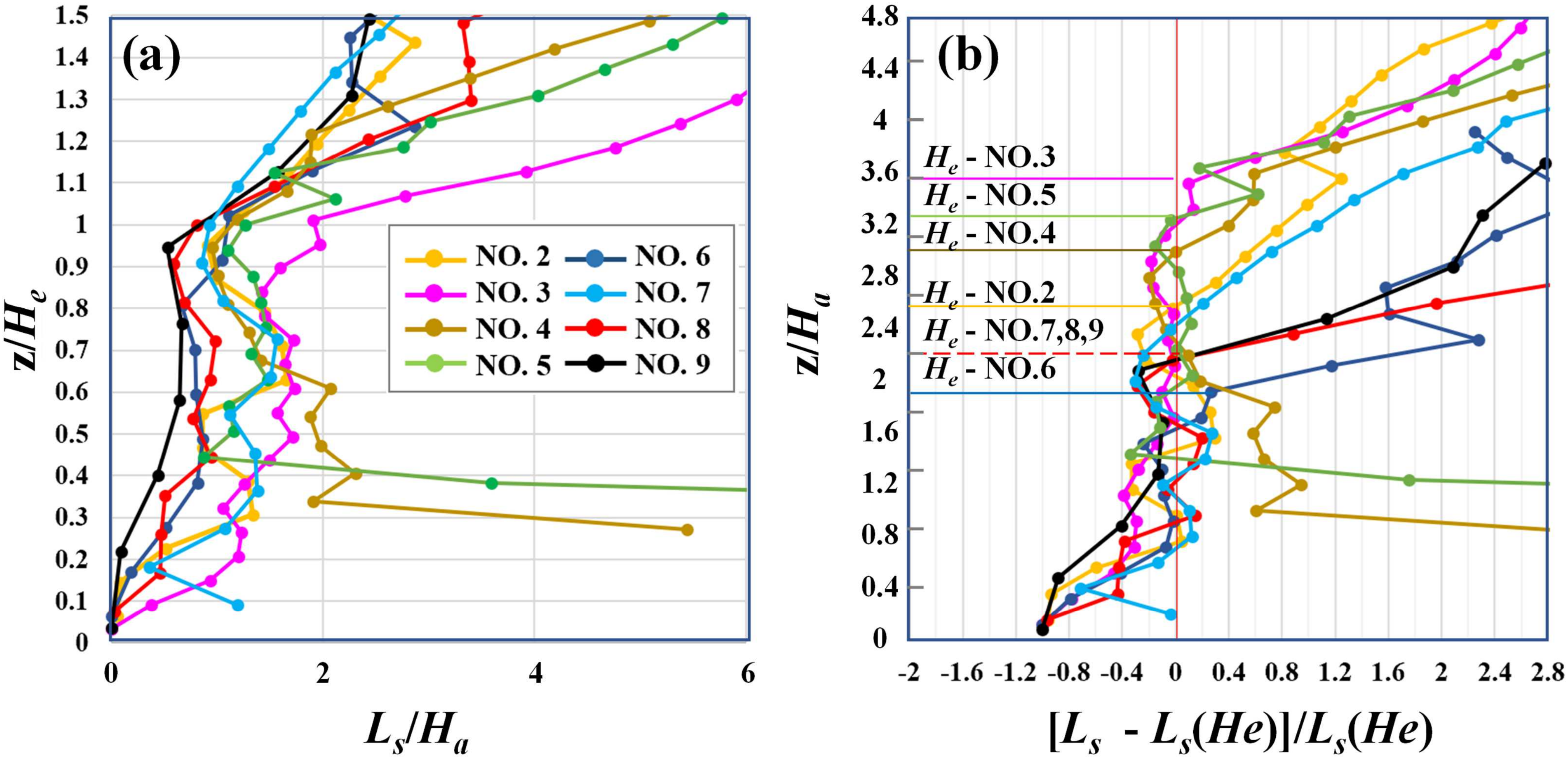

Fig. 6. Dimensionless profiles of (a) shear length scale L_s/H_a and (b) its difference compared with that at the UCL top $(L_s - L_s(H_e))/L_s(H_e)$ plotted against dimensionless height z/H_e and z/H_a, respectively.

400

Noticeably, d ranges where K_M reaches the first peak (i.e., the end point of K_M linearly increasing within the bottom UCLs) and the inflection height H_e (Fig. 5). The aerodynamic drag could be physically attributed to a shear layer, which is initiated around $z = H_e$ of an inflected wind profile, interacting with the underlying buildings. Such strong interaction is depicted as the aerodynamic drag centered at d. It falls below the inflection height (shear layer triggering) to a level where the ground effect ceases (the linear K_M ends; Eq. 5). Moreover, the eddy diffusivity is reduced abruptly in the vertical, which is likely due to the building blockage, thus disintegrating the shear layer into smaller eddies. Evidently, the form drag originates from the mixing-layer type dynamics. The drag-center-characterized shear layer acts as a transition partitioning the UCL from the ISL.

Eddies are mainly generated below the shear layer, especially in the bottom UCLs. They are modulated collectively by surface roughness and the mixing layer. This is not peculiar because, in such a dense, real urban morphology ($\lambda_p > 0.25$, a critical value defining the skimming flow regime; Reynolds and Castro, 2008), eddies are largely constrained within deep canopies (Zhao et al., 2020). This in turn enables the drag from the ground surface to have an effective impact. Nevertheless, the drag from the ground is not significant compared with its mixing-layer counterpart. Ignoring the mixing-layer effect would result in a noticeable deficit of momentum transport would appear (Fig. 4b).

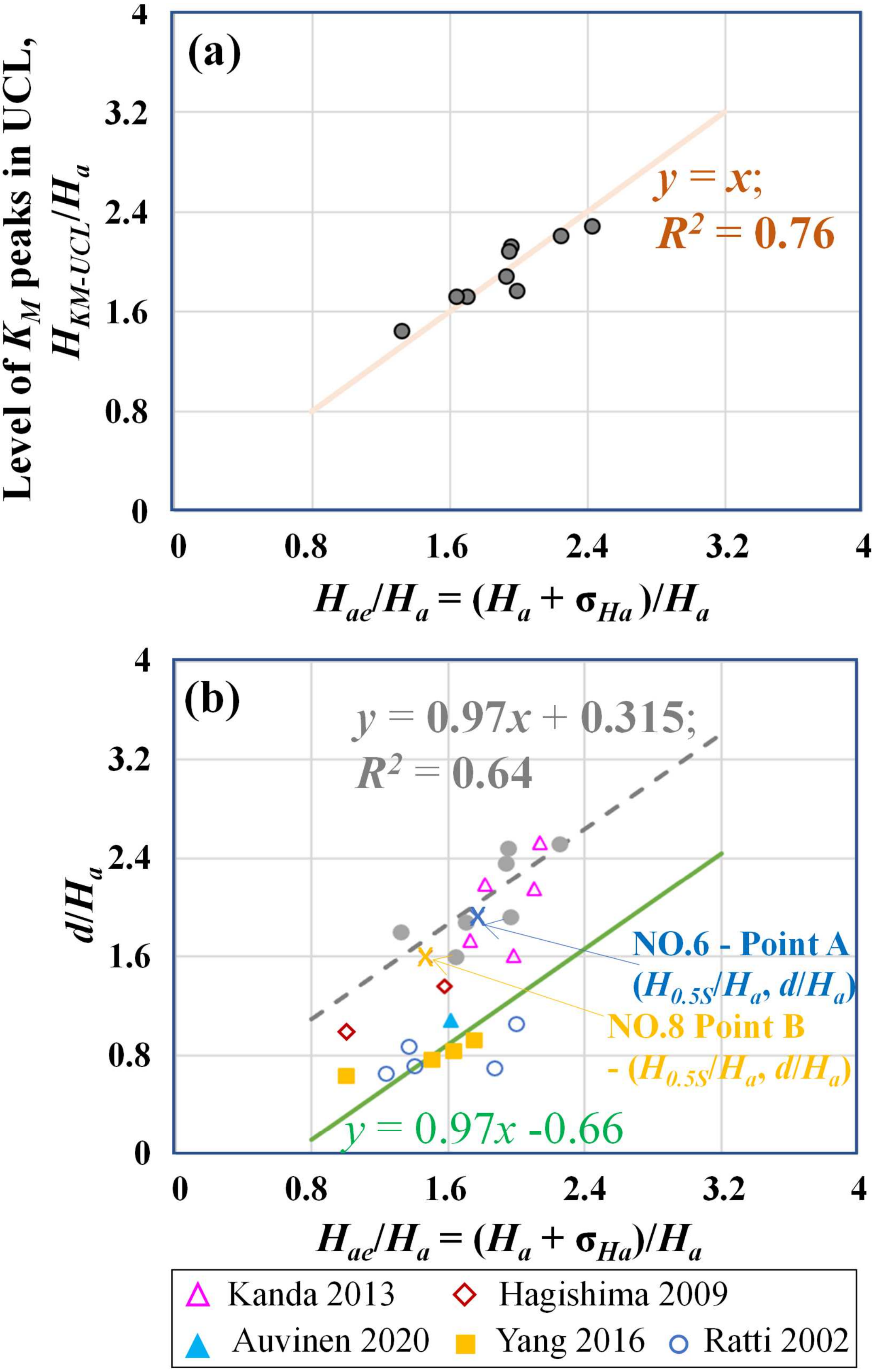

Fig. 7. Dimensionless (a) elevation of eddy diffusivity peaks $H_{KM\text{-}UCL}/H_a$ and (b) zero-plane displacement d/H_a plotted against height H_{ae}/H_a.

3.4.2 Characteristic height indicators of UCL flows

Within the UCL, the eddy diffusivity $K_{M\text{-}UCL}(z)$ peaks above the building roof level H_a in accordance with the characteristic building height H_{ae} as follows:

$$H_{ae} = H_a + \sigma_{H_a}. \tag{19}$$

The elevation of peaked eddy diffusivity $H_{K_{M-UCL}}/H_a$ and zero-plane displacement d/H_a of each subzone are plotted against H_{ae}/H_a in Fig.7. Noticeably, $H_{K_{M-UCL}}$ and d are highly correlated to H_{ae}. The zero-plane displacement d is slightly above H_{ae} (the coefficient of determination $R^2 = 0.64$), whereas the eddy diffusivity $K_{M\text{-}UCL}$ peaks at $z = H_{ae}$ ($R^2 = 0.76$). From the ground to $z = H_{K_{M-UCL}}$, the linear increasing $K_{M\text{-}UCL}$ (Eq. 5) well predicts the eddy diffusivity, as does the newly proposed mixing-length model (Eq. 13 and Fig. 4a). Beyond the linearly increasing $K_{M\text{-}UCL}$, the ground effect on the eddies diminishes and the $l_{m\text{-}UCL}$ model (Eq. 13) ceases to be valid hereabove. At $z = H_{K_{M-UCL}}$, the characteristic eddy size is not the largest because the mixing length generally peaks in the lower UCL (Fig. 4a). In contrast, the eddies facilitate the transport of substantial momentum due to the sharp velocity gradient in the vicinity of strong shear. Slightly above $z = H_{ae}$, the turbulence is intensified within the envelope of the strong shear layer initiated at the UCL top, signifying the level of aerodynamic drag. Therefore, H_{ae} serves as an aerodynamically effective roof level of ASL. The ground-surface resistance ceases at $z = H_{ae}$, whereas the eddy-driven momentum transport is amplified immediately above this level.

Apart from the bulky indicators of inflection height H_e and the drag center d, the flow dynamics could be quantified by the skewness of the streamwise fluctuating velocity *Su* (refer to Yao et al., 2022 for the mathematical equations). The maximum *Su* signifies substantial streamwise deceleration and rapid, intermittent flows. It occurs at the level $z = H_{Su}$ which is well correlated with the drag center (R^2 = 0.83; Fig. 8). Hence, UCL flows decelerate most around the aerodynamic drag center.

To measure the influence of building heterogeneity on the turbulence dynamics, the standard deviation of building height σ_{Ha} is used to describe the characteristic heights *d*, H_{Su} and H_e. Analogous to H_{ae}, three levels at $0.5\sigma_{Ha}$, $1.5\sigma_{Ha}$, and $2\sigma_{Ha}$ above the building roof (H_a) are defined by

$$H_{0.5S} = H_a + 0.5\sigma_{H_a}, \tag{20}$$

$$H_{1.5S} = H_a + 1.5\sigma_{H_a} \tag{21}$$

and

$$H_{2S} = H_a + 2\sigma_{H_a}, \tag{22}$$

respectively. In most of the subzones, S_u peaks above H_{ae}, correlating well with $H_{1.5S}$ (R^2 = 0.66; Fig. 9a). With the weakening influence from the ground surface above H_{ae} (stronger shear-layer effect), the majority flows that present the peaked *Su* at $H_{1.5S}$ decelerate. Concurrently, the large eddies wrapped in the shear layer cascade into smaller ones (Fig. 4a). The strong shear layer initiated around the UCL top at $z = H_e$ is physically located at approximately $0.5\sigma_{Ha}$ above the peak *Su* (i.e., $H_e = H_{Su} + 0.5\sigma_{Ha}$). The linear regression $H_e = H_{2S}$ well predicts the relationship between the two heights (R^2 = 0.82; Fig. 9b).

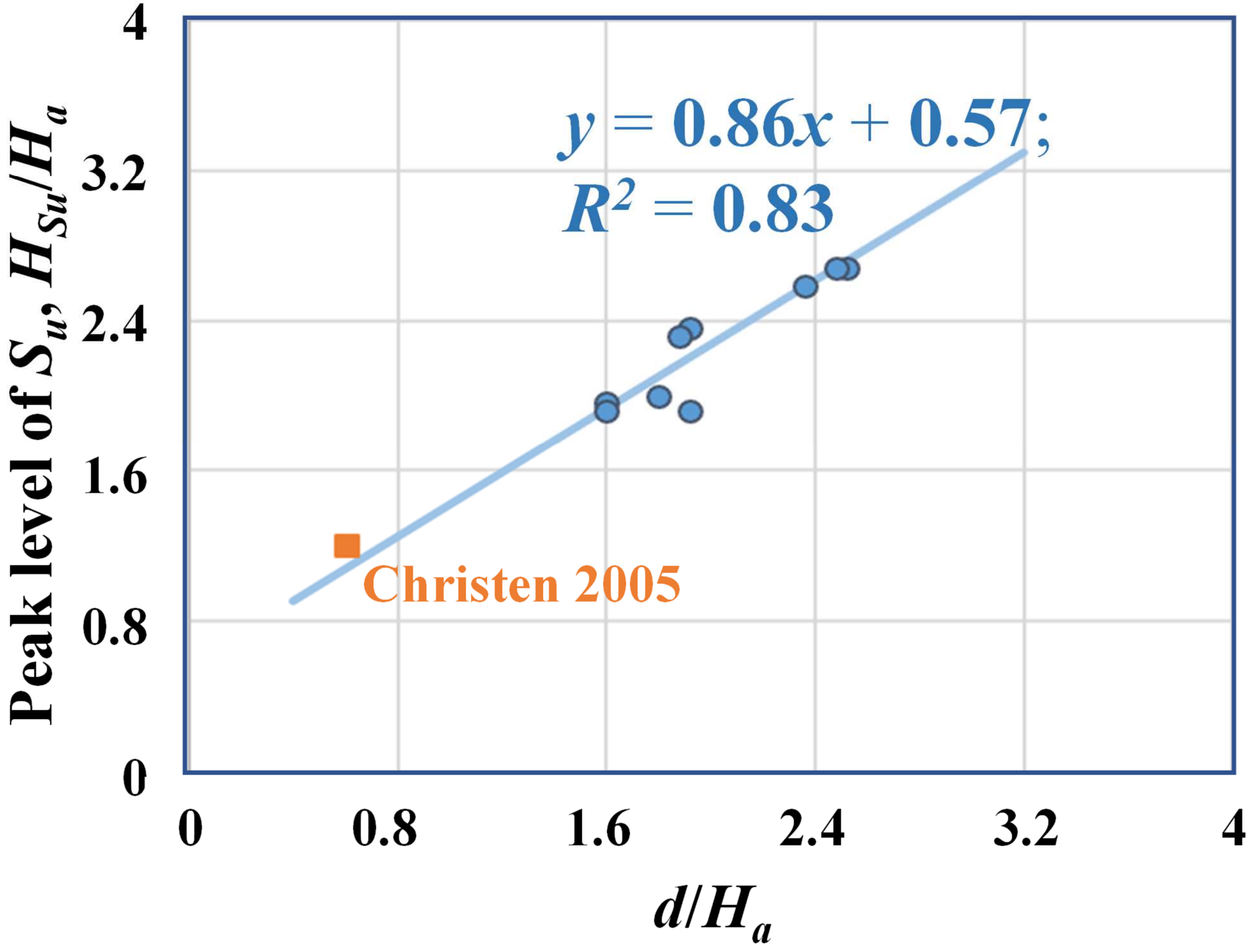

Fig. 8. Dimensionless elevation of peaked skewness of streamwise velocity H_{Su}/H_a plotted against zero-plane displacement d/H_a.

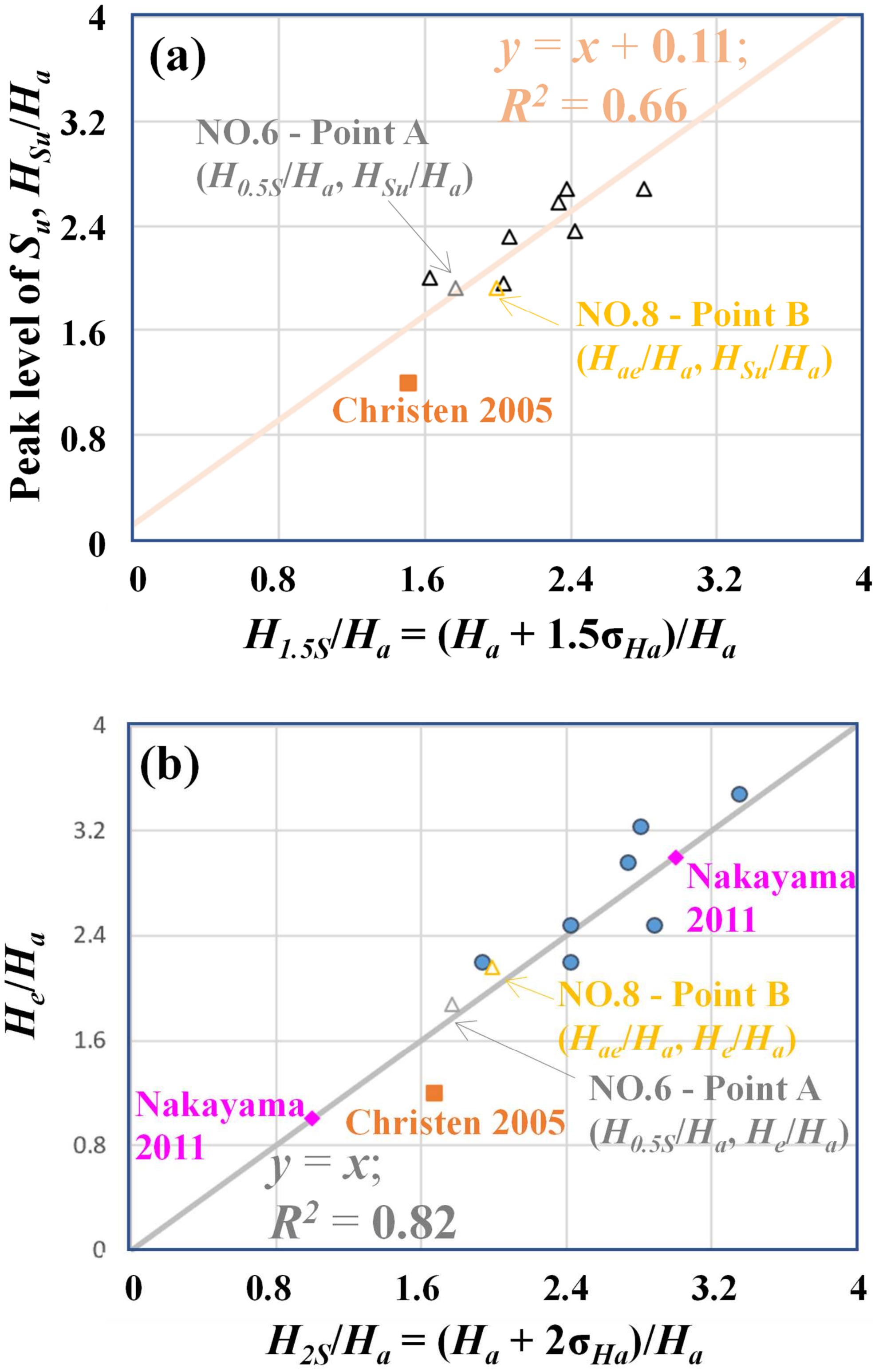

Fig. 9. Dimensionless profiles of (a) elevation of peaked skewness H_{Su}/H_a plotted against $H_{1.5S}/H_a$ and (b) inflection height H_e/H_a plotted against H_{2S}/H_a.

Note that in the regression of d, H_{Su}, and H_e (Fig. 7b and 9), a smaller portion of height variation is used in subzones NO.6 (σ_{Ha}/H_a = 1.2) and NO.8 (σ_{Ha}/H_a = 1.1) because of the buildings of the two subzones are distinctly diversified compared to others. Their drag centers are lower relative to their substantial building height variation, i.e., $d \approx H_{0.5S}$ (Fig. 7b). For NO.6, in which the building height is the most diversified (K_h > 8), the three characteristic heights (d, H_{Su}, and H_e) are located close to each other ($H_{0.5S}$; Fig. 9). For NO.8, the Su peak and the inflection are located at the aerodynamic roof level H_{ae}. Therefore, the building height diversity promotes shear vertically (i.e., higher H_{ae}). The core dynamics is restrained in a thin layer regardless of the large height variation. A more heterogeneous surface tends to lower its drag center and results in a shallower (compared with its broad height spectra) vertical zone of strong dynamics.

The linear regression models (Fig. 7–9) reveal the importance of building height heterogeneity, as evaluated using σ_{Ha}, for the generation of characteristic eddies, the production of shear, and turbulence dynamics. The relationship between d and H_{ae} (i.e., $\sigma_{Ha} + H_a$) of the current urban surfaces is supported by Kanda et al. (2013) (i.e., the urban cases are *ID10*, *60*, *63*, *96*, *97*). Figure 7b also shows the datasets of Yang et al. (2016) (i.e., cases *L25S* and *Lf25S*), Ratti et al. (2002) (i.e., London, Toulouse, Berlin, Salt Lake City, Los Angeles), and Auvinen et al. (2020) (i.e., domain Ω*(3)*). The figure indicates that a smaller building heterogeneity provokes a lower drag center d, and a moderate heterogeneity induces the aerodynamic drag centered around H_{ae} (cases *ST1.5-sq* and *SQ1.5* of Hagishima et al., 2009). The vertical profile of linear eddy diffusivity is partitioned into three segments: ISL ($z \geq H_{2S}$), the lower UCL ($z \leq$

H_{ae}; Fig. 5), and the thin layer (with a thickness of σ_{Ha}) where strong mixing dominates. Therefore, the majority of ASL flows decelerate (H_{Su}) and the core drag (d) occurs around $z = H_{1.5S}$. The abrupt decelerations around H_{Su} (i.e., $2\sigma_{Ha} + H_a$) are also found in the winds measured over Basel (Christen, 2005), and urban-like roughness elements (Nakayama et al., 2011) (Figure 9). Therefore, a model of these characteristic heights for turbulence quantities is conceived, in which the UCL and ISL winds are expressed as the exp-law and the log-law, respectively, in line with the aforementioned dynamics.

3.5 Effects of urban surface heterogeneity on the characteristic length scale of eddies

In this section, the shear length scale $L_{s\text{-}ML}$ (= H_e/α; Eq. 10) is used to diagnose the length scale of dominant eddies in the shear layer around the UCL top. The LES datasets are used to reveal the relationship between the eddy size and the bulk-flow indicators for momentum transport (e.g., u_*) and mean-wind-decay rate (e.g., α). Further, the roles of building height and urban heterogeneity in determining the characteristic eddy size are investigated.

Fig. 10a shows that, normalized by H_a, $L_{s\text{-}ML}$ is inversely proportional to α ($R^2 = 0.8$). Notably, that both the height and plan area of each building (i.e., building volume) are used to calculate the area-weighted average building height H_a. The figure indicates that eddies with a larger length scale generated by an equivalent volume of buildings promote turbulent mixing vertically. Subsequently, the wind decay slows toward the UCLs, leading to a more uniform vertical profile of UCL mean-wind speed (Fig. 3b). Using σ_{Ha} to normalize $L_{s\text{-}ML}$ instead, the correlation between $L_{s\text{-}ML}$ and α is further enhanced ($R^2 = 0.9$; Fig. 10b). For the same degree of height variation, a larger shear length scale also lessens the wind decay.

Because of the noticeable building heterogeneity ($K_h > 5$) in subzones NO.6 and NO.8, UCL wind attenuation slows. The attenuation coefficient α is thus reduced, resulting in the data points deviating significantly from the linear regression (Fig. 10a). The discrepancy is likely attributed to the clusters of skyscrapers (extreme H_a). Because of their large height standard deviation, which composes a distinct urban morphology that is above (below) the diagonal $\sigma_{Ha}/H_a = 1$ ($L_{s\text{-}ML}/\sigma_{Ha} = 1$) in Fig. 10c (Fig. 10d), only half of the subzones, NO.6 and NO.8, are used to develop the regression model (Fig. 10b). In contrast, the rest possess a similar morphological pattern, with higher building volume tending to promote height diversity despite the irregular building layout in the current real urban morphology. Regardless of the appreciable building heterogeneity of NO.1 ($\lambda_p \approx 0.7$; $\sigma_{Ha}/H_a = 0.89$), the shear length scale is greatly shortened because of the extremely dense built pattern. Excluding the three subzones mentioned above, the shear length scale could be correlated well with σ_{Ha} for the linear regression $L_{s\text{-}ML} = 2.11\sigma_{Ha} - 12.09$ ($R^2 = 0.84$, Fig. 10d).

A second-order polynomial characterizes well the shear length scale L_s in terms of the friction velocity u_* ($R^2 = 0.75$, Fig. 11a). It in turn indicates that larger eddies (longer L_s) are generated at the UCL top, provoking the turbulent transport of more momentum flux and resulting in rougher surfaces (larger u_*). Fig. 11b shows that u_* is inversely proportional to α ($R^2 = 0.86$), so rougher surfaces feature more uniform UCL winds with a slower decay rate toward the UCLs, which is in line with cases of Yang et al. (2016) (i.e., *L25S*, *L25A*, *L11S*, and *L11A*). Moreover, the longer L_s indicates the amplified shielding from the shear layer initiated at the UCL top, which is extended to deeper canopies (Fig. 6). Note that the mark representing subzone NO.1 deviates beyond the linear function (Fig. 11b). This suggests that the resistance to the prevailing winds is not small when α is largest. In this subzone, the heterogeneous buildings (σ_{Ha}/H_a = 0.89) exert appreciable resistance to the winds. In view of its largest packing density ($\lambda_p \approx 0.7$), the flows in NO.1 penetrate shallowly into the UCLs and the winds quickly abate during descent.

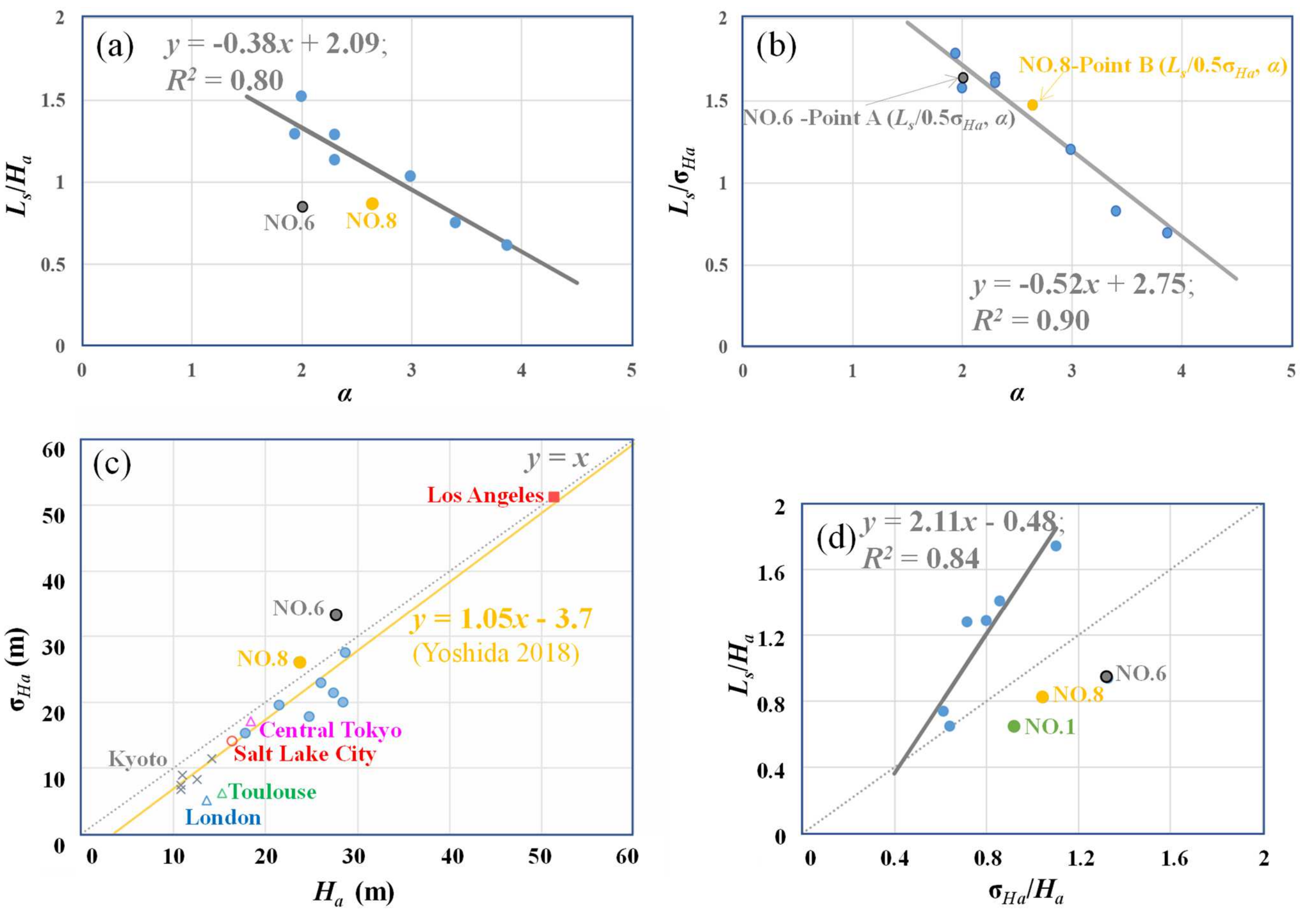

Fig. 10. Dimensionless (a) shear length scale $L_s/H_a = H_e/(\alpha H_a)$ and (b) $L_s/\sigma_{Ha} = H_e/(\alpha\sigma_{Ha})$ plotted against attenuation coefficient α. (c) Building height standard deviation σ_{Ha} plotted against area-weighted average building height H_a. (d) Dimensionless shear length scale L_s/H_a plotted against dimensionless building height standard deviation σ_{Ha}/H_a.

534

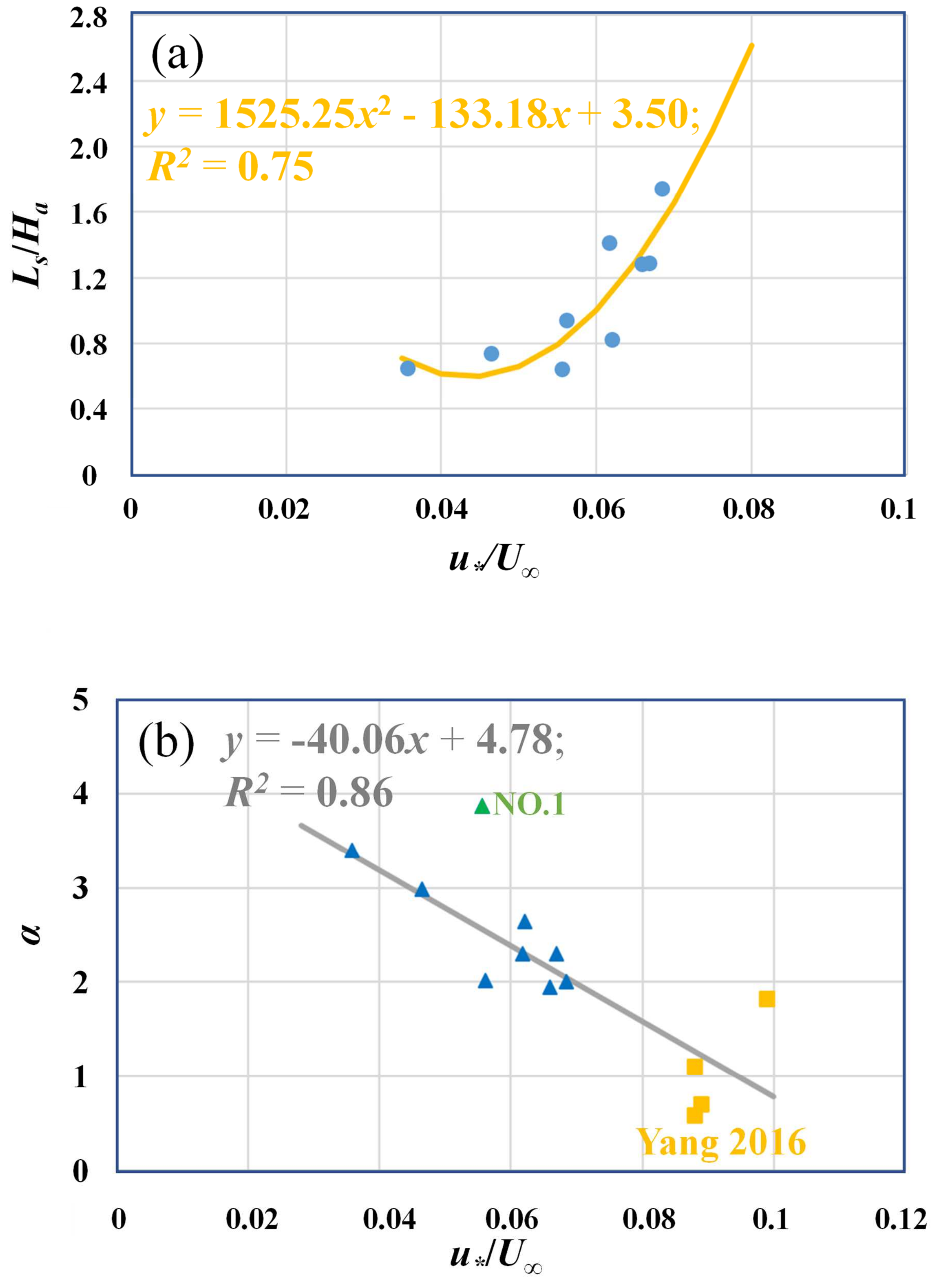

Fig. 11. Dimensionless (a) shear length scale L_s/H_a (= H_e/α) and (b) attenuation coefficient α plotted against friction velocity u_*/U_∞.

4. Discussion

In this study, a linear function of eddy diffusivity of turbulent momentum flux K_M and the exponential function of wind profile are tailored to the UCL flows over real urban morphologies. The mixing-length l_m model that fosters the modeling of UCL eddy generation and organization is thus developed. It is constructed with physical bases, that is, the drag from ground surfaces and the shear from ASL-building interactions. In response to ground surfaces, eddies are organized in a self-similar manner analogous to the standard ASL (Townsend 1996). In contrast, for the shear-driven mixing-layer flows, eddies whose shear length scale are independent of height are rather identical. Thus, the eddy diffusivity K_M increases linearly with increasing height.

Eddies grow from the ground until l_m peaks in the lower UCLs. With the influence from the ground surface decreasing with height, eddies are induced by the UCL top, so shear gradually dominates. In this connection, the upper endpoint of the linear K_M is determined as the aerodynamic effective roof level H_{ae} for real urban areas which corroborates to $H_a + \sigma_{Ha}$. Within the strong shear layer, the turbulence fluctuations are amplified, as denoted by the maximum S_u being located around $z = H_{ae} + 0.5\sigma_{Ha}$. While the UCL-top shear alleviates this effect, the self-similar eddy organization resumes in ISL. The linear K_M increases faster than its UCL counterpart. Such eddy orientation lays the foundation for the parameterizations of UCL turbulence quantities.

The shear length scale persists into the deep canopies, as predicted by the model at UCL top, establishing the shear-characterized UCL flows analogously to those of the mixing-layer regime. Moreover, discarding shear would result in a large turbulent momentum flux deficit. This proves the necessity of considering the mixing-layer shear in the parametrization of turbulence quantities. The exp-law captures the shear strength of the UCL-ISL interface well. Further, the mixing-length model performs well at lower UCLs, especially the elevation of peak l_m. This demonstrates that the breakdown of assumptions for the exp-law is not necessarily adequate for its non-transferability from porous canopies to real urban areas. Unlike the invariant drag coefficient C_d and mixing length l_m of porous-media canopies, this paper confirms the validity of the exp-law for urban canopies despite the inherent difference between the two types of canopies (Finnigan, 2000). The novel parametrizations fill the gap of the ASL flows over real, dense cities, which is beneficial to climate application and UCM constructions.

UCL-top shear is crucial in determining the MWS profiles and the turbulence dynamics in the canopies beneath. Generally, a larger shear length scale manifests a rougher surface. Hence, larger characteristic eddies promote UCL turbulent mixing, leading to more uniform UCL winds and a smaller wind decay rate α. The surface roughness is likely to be augmented by the diverse building height distribution. However, the deficient turbulence structures could lead to minor momentum flux loss due to the excessive blockage from the upper parts of the facades in the exceptional heterogeneous urban areas.

The parameterizations of UCL flows proposed in this study are tailored for the specific urban surfaces in Hong Kong that exhibit large building height varieties ($\sigma_{Ha}/H_a \geqslant 0.7$) and mostly compact built layouts ($\lambda_p > 0.35$). Note that the urban morphologies of other cities, including the building configurations (e.g., density and height distribution) and layouts (e.g., open main streets and the distribution of high-rises), vary case by case. The transferability of the current parametrizations of UCL flows to other types of surface morphologies, such as the dense low-rise packed layout (e.g., $\lambda_p \approx 0.55$ of London, $\lambda_p \approx 0.4$ of Toulouse) (Ratti et al., 2002), and the open high-rise area (e.g., $\lambda_p \approx 0.28$, $\sigma_{Ha} \approx H_a$ of Los Angles) (Fig. 10c), is of great interests to investigate.

With that, the ideas and procedures that formulate the current UCL model could be extended in future studies on diverse real urban topologies. Moreover, if the urban surface could be properly characterized and quantified, such as in megacities with a comparable building height variability to the average building height in Fig. 10c (Yoshida et al., 2018), a rich dataset of the UCL flow parameters outfitting all kinds of urban morphologies could be established. Likewise, the proposed UCL model contributes to the database for the construction of the UCMs, which will be beneficial to the meteorological applications.

5. Conclusions

UCL flows over real urban morphology are analogous to a plane-mixing-layer analogy and are characterized by exponential MWS profiles. A model is proposed by considering the collective effect of the ground surface and shear layer at the UCL top on the eddy organization within the canopies. The evaluation of the model is conducted via the remarkable parameterizations of the mixing length and the turbulent momentum flux. The exponential law characterizes the UCL winds for real, dense urban areas. A smaller attenuation coefficient manifests a rougher surface due to eddy generation with larger shear length scales. The characteristic eddies enrich momentum transport and turbulence mixing, leading to more uniform UCL winds. The results indicate that building height heterogeneity is indicative of the roughness degree of real urban morphology. The stronger UCL winds and the more efficient momentum transport by rougher surfaces promote aged air removal from urban areas.

Acknowledgment

This research is conducted in part using the research computing facilities and/or advisory services offered by Information Technology Services (ITS), The University of Hong Kong (HKU). Technical support from Ms. Lilian Y.L. Chan, Mr. W.K. Kwan, Mr. Bill H.T. Yau, and Mr. Juilian Yeung is appreciated. This study is partly supported by the Hong Kong (HK) Research Grants Council (RGC) Theme-based Research Scheme (TRS)T24-504/17-N, the RGC Collaborative Research Fund (CRF) C7064-18G, RGC CRF C5108-20G as well as the RGC General Research Fund (GRF) 17209819 and 17211322.

References

Alwi, A., Mohamad, M.F., Ikegaya, N. and Abd Razak, A., 2023. Effect of protruding eave on the turbulence structures over two-dimensional semi-open street canyon. Building and Environment, 228, pp.109921.

Auvinen, M., Boi, S., Hellsten, A., Tanhuanpää, T. and Järvi, L., 2020. Study of realistic urban boundary layer turbulence with high-resolution large-eddy simulation. Atmosphere, 11(2), p.201.

Böhm, M., Finnigan, J.J., Raupach, M.R. and Hughes, D., 2013. Turbulence structure within and above a canopy of bluff elements. Boundary-Layer Meteorology, 146(3), pp.393-419.

Brunet, Y., 2020. Turbulent flow in plant canopies: historical perspective and overview. Boundary-Layer Meteorology, 177(2), pp.315-364.

Castro, I.P., 2017. Are urban-canopy velocity profiles exponential?. Boundary-Layer Meteorology, 164(3), pp.337-351.

Castro, I.P., Cheng, H. and Reynolds, R., 2006. Turbulence over urban-type roughness: deductions from wind-tunnel measurements. Boundary-Layer Meteorology, 118, pp.109-131.

Cheng, H. and Castro, I.P., 2002. Near-wall flow over urban-type roughness. Boundary-Layer Meteorology, 104(2), pp.229–259.

Cheng, W.C., Liu, C.-H., Ho, Y.-K., Mo, Z., Wu, Z., Li, W., Chan, L.Y.L., Kwan, W.K., Yau, H.T., 2021. Turbulent flows over real heterogeneous urban surfaces: Wind tunnel experiments and Reynolds-averaged Navier-Stokes simulations. Building Simulation, 14, pp. 1345–1358.

Cheng, W.C. and Porté-Agel, F., 2021. A Simple Mixing-Length Model for Urban Canopy

Flows. Boundary-Layer Meteorology, 181(1), pp.1-9.

Cheng, W.C. and Yang, Y., 2022. Scaling of Flows Over Realistic Urban Geometries: A Large-Eddy Simulation Study. Boundary-Layer Meteorology, pp.1-20.

Christen, A., 2005. Atmospheric turbulence and surface energy exchange in urban environments: results from the Basel Urban Boundary Layer Experiment (BUBBLE) (Doctoral dissertation, University_of_Basel).

Elbing, B.R., Solomon, M.J., Perlin, M., Dowling, D.R. and Ceccio, S.L., 2011. Flow-induced degradation of drag-reducing polymer solutions within a high-Reynolds-number turbulent boundary layer. Journal of Fluid Mechanics, 670, pp.337-364.

Feigenwinter, C. and Vogt, R., 2005. Detection and analysis of coherent structures in urban turbulence. Theoretical and applied climatology, 81, pp.219-230.

Finnigan, J., 2000. Turbulence in plant canopies. Annual Review of Fluid Mechanics, 32(1), pp.519-571.

Ghisalberti, M. and Nepf, H.M., 2002. Mixing layers and coherent structures in vegetated aquatic flows. Journal of Geophysical Research: Oceans, 107(C2), pp.3-1.

Ghisalberti, M. and Nepf, H., 2006. The structure of the shear layer in flows over rigid and flexible canopies. Environmental Fluid Mechanics, 6(3), pp.277-301.

Giometto, M.G., Christen, A., Meneveau, C., Fang, J., Krafczyk, M. and Parlange, M.B., 2016. Spatial characteristics of roughness sublayer mean flow and turbulence over a realistic urban surface. Boundary-Layer Meteorology, 160(3), pp.425-452.

Hagishima, A., Tanimoto, J., Nagayama, K. and Meno, S., 2009. Aerodynamic parameters of regular arrays of rectangular blocks with various geometries. Boundary-Layer

Meteorology, 132, pp.315-337.

Han, B.S., Park, S.B., Baik, J.J., Park, J. and Kwak, K.H., 2017. Large-eddy simulation of vortex streets and pollutant dispersion behind high-rise buildings. Quarterly Journal of the Royal Meteorological Society, 143(708), pp.2714-2726.

He, Y., Tablada, A. and Wong, N.H., 2019. A parametric study of angular road patterns on pedestrian ventilation in high-density urban areas. Building and environment, 151, pp.251-267.

Hommema, S.E. and Adrian, R.J., 2003. Packet structure of surface eddies in the atmospheric boundary layer. Boundary-Layer Meteorology, 106, pp.147-170.

Huq, P., White, L.A., Carrillo, A., Redondo, J., Dharmavaram, S. and Hanna, S.R., 2007. The shear layer above and in urban canopies. Journal of Applied Meteorology and Climatology, 46(3), pp.368-376.

Kanda, M., Inagaki, A., Miyamoto, T., Gryschka, M. and Raasch, S., 2013. A new aerodynamic parametrization for real urban surfaces. Boundary-layer meteorology, 148(2), pp.357-377.

Leonardi S. and Castro I.P., 2010. Channel flow over large roughness: a direct numerical simulation study. Journal of Fluid Mechanics, 651, pp.519-539.

Li, P. and Wang, Z.H., 2020. Modeling carbon dioxide exchange in a single-layer urban canopy model. Building and Environment, 184, pp.107243.

Li, Q., Yang, J. and Yang, L., 2021. Impact of urban roughness representation on regional hydrometeorology: An idealized study. Journal of Geophysical Research: Atmospheres, 126(4), pp.e2020JD033812.

Li, X.X., Liu, C.-H., and Leung, D.Y.C., 2008. Large-eddy simulation of flow and pollutant dispersion in high-aspect-ratio urban street canyons with wall model. Boundary-Layer Meteorology, 129(2), pp. 249-268.

Liu, Y., Liu, C.-H., Brasseur, G.P., and Chao, C.Y.H., 2023a. Wavelet analysis of the atmospheric flows over real urban morphology. Science of the Total Environment, 859, 160209.

Liu, Y., Liu, C.-H., Brasseur, G.P., and Chao, C.Y.H., 2023b. Proper orthogonal decomposition of large-eddy simulation data over real urban morphology. Sustainable Cities and Society, 89, 104324.

Lu, L. and Sun, K., 2014. Wind power evaluation and utilization over a reference high-rise building in urban area. Energy and Buildings, 68, pp.339-350.

Macdonald, R.W., 2000. Modelling the mean velocity profile in the urban canopy layer. Boundary-Layer Meteorology, 97(1), pp.25-45.

Mathis, R., Hutchins, N. and Marusic, I., 2009. Large-scale amplitude modulation of the small-scale structures in turbulent boundary layers. Journal of Fluid Mechanics, 628, pp.311-337.

Mei, S.J. and Yuan, C., 2022. Urban buoyancy-driven air flow and modelling method: A critical review. Building and Environment, 210, pp.108708.

Mo, Z. and Liu, C.-H., 2023. Inertial and roughness sublayer flows over real urban morphology: A comparison of wind tunnel experiment and large-eddy simulation. Urban Climate, 49, 101530.

Monin, A.S. and Obukhov, A.M., 1954. Osnovnye zakonomernosti turbulentnogo peremeshivanija v prizemnom sloe atmosfery (Basic laws of turbulent mixing in the atmosphere near the ground). Trudy geofiz. inst. AN SSSR, 24(151), pp.163-187.

Nagel, T., Schoetter, R., Bourgin, V., Masson, V. and Onofri, E., 2023. Drag Coefficient and Turbulence Mixing Length of Local Climate Zone-Based Urban Morphologies Derived Using Obstacle-Resolving Modelling. Boundary-Layer Meteorology, 186(3), pp.737-769.

Nakayama, H., Takemi, T. and Nagai, H., 2011. LES analysis of the aerodynamic surface properties for turbulent flows over building arrays with various geometries. Journal of Applied Meteorology and Climatology, 50(8), pp.1692-1712.

Nezu, I. and Sanjou, M., 2008. Turburence structure and coherent motion in vegetated canopy open-channel flows. Journal of Hydro-Environment Research, 2(2), pp.62-90.

Novak, M.D., Warland, J.S., Orchansky, A.L., Ketler, R. and Green, S., 2000. Wind tunnel and field measurements of turbulent flow in forests. Part I: uniformly thinned stands. Boundary-Layer Meteorology, 95(3), pp.457-495.

OpenFOAM, OpenFOAM, The OpenFOAM Foundation, 2021. https://openfoam.org/.

Park, S.B., Baik, J.J. and Lee, S.H., 2015. Impacts of mesoscale wind on turbulent flow and ventilation in a densely built-up urban area. Journal of Applied Meteorology and Climatology, 54(4), pp.811-824.

Poggi, D., Porporato, A., Ridolfi, L., Albertson, J.D. and Katul, G.G., 2004. The effect of vegetation density on canopy sub-layer turbulence. Boundary-Layer Meteorology, 111(3), pp.565-587.

Ratti, C., Di Sabatino, S., Britter, R., Brown, M., Caton, F. and Burian, S., 2002. Analysis of 3-

D urban databases with respect to pollution dispersion for a number of European and American cities. Water, Air and Soil Pollution: Focus, 2, pp.459-469.

Raupach, M. and Thom, A.S., 1981. Turbulence in and above plant canopies. Annual Review of Fluid Mechanics, 13(1), pp.97-129.

Raupach, M.R., Finnigan, J.J. and Brunet, Y., 1996. Coherent eddies and turbulence in vegetation canopies: the mixing-layer analogy. Boundary-Layer Meteorology 25th Anniversary Volume, 1970–1995: Invited Reviews and Selected Contributions to Recognise Ted Munn's Contribution as Editor over the Past 25 Years, pp. 351-382.

Reynolds, R.T. and Castro, I.P., 2008. Measurements in an urban-type boundary layer. Experiments in Fluids, 45(1), pp.141-156.

Schmidt, W., 1925. Der Massenaustausch in freier Luft und Verwandte Erscheinungen. Problem der Kosmischen Physics, Hamburg, Verlag Von Henri Grand, 176.

Smagorinsky, J., 1963. General circulation experiments with the primitive equations: I. The basic experiment. Monthly Weather Review, 91(3), pp.99-164.

Theeuwes, N.E., Ronda, R.J., Harman, I.N., Christen, A. and Grimmond, C.S.B., 2019. Parametrizing horizontally-averaged wind and temperature profiles in the urban roughness sublayer. Boundary-Layer Meteorology, 173(3), pp.321-348.

Thom, A.S., 1971. Momentum absorption by vegetation. Quarterly Journal of the Royal Meteorological Society, 97(414), pp.414-428.

Thomas, C. and Foken, T., 2007. Organised motion in a tall spruce canopy: temporal scales, structure spacing and terrain effects. Boundary-Layer Meteorology, 122, pp.123-147.

Tominaga, Y., Mochida, A., Yoshie, R., Kataoka, H., Nozu, T., Yoshikawa, M. and Shirasawa, T., 2008. AIJ guidelines for practical applications of CFD to pedestrian wind environment around buildings. Journal of Wind Engineering and Industrial Aerodynamics, 96(10-11), pp.1749-1761.Vinayak, B., Lee, H.S., Gedam, S., and Latha, R., 2022. Impacts of future urbanization on urban microclimate and thermal comfort over the Mumbai metropolitan region, India. Sustainable Cities and Society, 79, 103703.

Wong, C.C.C. and Liu, C.-H., 2013. Pollutant plume dispersion in the atmospheric boundary layer over idealized urban roughness. Boundary-Layer Meteorology, 147, pp. 281-300.

Wu, Z. and Liu, C.-H., 2018. Source depletion analogy for reactive plume dispersion over schematic urban areas. Atmospheric Environment, 190, pp.226-231.

Xie Z.T., Coceal O, Castro IP., 2008. Large-eddy simulation of flows over random urban-like obstacles. Boundary-Layer Meteorology, 129, pp.1–23.

Xie Z.T. and Castro I.P., 2009. Large-eddy simulation for flow and dispersion in urban streets. Atmospheric Environment 43(13), pp.2174–2185.

Yang, X.I., Sadique, J., Mittal, R. and Meneveau, C., 2016. Exponential roughness layer and analytical model for turbulent boundary layer flow over rectangular-prism roughness elements. Journal of Fluid Mechanics, 789, pp.127-165.

Yao, L., Liu, C.H., Mo, Z., Cheng, W.C., Brasseur, G.P. and Chao, C.Y., 2022. Statistical analysis of the organized turbulence structure in the inertial and roughness sublayers over real urban area by building-resolved large-eddy simulation. Building and Environment, 207, pp.108464.

Yoshida, T., Takemi, T. and Horiguchi, M., 2018. Large-eddy-simulation study of the effects of building-height variability on turbulent flows over an actual urban area. Boundary-

Layer Meteorology, 168(1), pp.127-153.

Zhao, H.Q., Wang, W.J., Zhao, Y.F., Liu, X.B., Chou, Q.C. and Gao, Y., 2023. New hyperbolic tangent formula for mixing layer in vegetated flow. Journal of Hydrology, pp.129061.

Zhao, Y., Chew, L.W., Kubilay, A. and Carmeliet, J., 2020. Isothermal and non-isothermal flow in street canyons: A review from theoretical, experimental and numerical perspectives. Building and Environment, 184, pp.107163.

Zhu, X., Iungo, G.V., Leonardi, S. and Anderson, W., 2017. Parametric study of urban-like topographic statistical moments relevant to a priori modelling of bulk aerodynamic parameters. Boundary-Layer Meteorology, 162(2), pp.231-253.

Zou, J., Zhou, B. and Sun, J., 2017. Impact of eddy characteristics on turbulent heat and momentum fluxes in the urban roughness sublayer. Boundary-Layer Meteorology, 164(1), pp.39-62.